On turbulence closures for two-phase sediment-laden flow models

J. Chauchat, S. Guillou

On turbulence closures for two-phase sediment-laden flow models

Julien Chauchat[1] and Sylvain Guillou[2]

Received 20 December 2007; revised 11 July 2008; accepted 18 August 2008; published 20 November 2008.

[1] Recent experimental studies show that there exists a difference between horizontal velocity components of particles and of fluid in sediment-laden open channel flows. For suspended particles with sufficient inertia, volume fraction profile cannot be represented without the introduction of empirical parameters in passive scalar sediment transport models. The aim of this paper is to propose a two-phase model that allows representation of the main features of sediment-laden flows: the existence of a horizontal velocity difference between particles and fluid, the dispersion of particles by fluid turbulent motion, and the damping of fluid turbulent kinetic energy. A 2-D vertical numerical model for suspended particle transport in open channels using a two-phase approach is used in conjunction with experimental measurements. Different turbulence models for both phases are presented. The fluid phase turbulence is modeled by a $k - \varepsilon$ model. Two models for the solid phase turbulence are used: a first-order model, based on the kinetic theory of granular flows, and an algebraic model based on an homogeneous, isotropic, and steady fluid turbulence assumption. We demonstrate that a modeling approach of the coupling between fluid and solid turbulence allows reproduction of the main features of sediment-laden flows. We show this approach represents an improvement compared with the classical approach. We show that a simple algebraic model based on the homogeneous, isotropic, and steady fluid turbulence assumption for the solid phase turbulence allows the physical phenomenon to be reproduced with very slight differences compared with a first-order model.

Citation: Chauchat, J., and S. Guillou (2008), On turbulence closures for two-phase sediment-laden flow models, *J. Geophys. Res.*, *113*, C11017, doi:10.1029/2007JC004708.

1. Introduction

[2] Sediments suspended in natural waters, rivers, estuaries or coasts, are transported by bed load and suspended load [*Fredsoe*, 1993]. Bed load is the part of the total load where sediment particles are in contact with the bed sediment and constrained by the effective shear stress. Suspended load is the part of the total load which is moving without continuous contact with the bed sediment as the result of the agitation of the fluid. In this paper we will focus our attention on the suspended sediment load. Historically, *Rouse* [1937] describe the suspended load by supposing that, at steady state, the gravitational vertical downward flux of particles $w_s c$ is balanced by a turbulent vertical upward flux of particles $\overline{w_s' c'}$:

$$\frac{\partial w_s c}{\partial z} + \frac{\partial \overline{w_s' c'}}{\partial z} = 0, \tag{1}$$

where w_s, w_s', c, c' represent, respectively, the sediment particle settling velocity and its fluctuating component, and the sediment particle concentration and its fluctuating component. z designate the vertical coordinate and the overbar represents averaging over time.

[3] In the Rouse approach the turbulent vertical upward flux of particles is modeled with the eddy viscosity concept as:

$$\overline{w_s' c'} = \nu_f^t \frac{\partial \overline{c}}{\partial z} \tag{2}$$

[4] Given a closure for the eddy viscosity vertical profile (3) and a reference concentration c^a at a given adimensionalized height above the bed σ^a it is possible to solve analytically equation (1) to obtain the vertical concentration profile (4).

$$\nu_f^t = \kappa u_* \sigma h (1 - \sigma) \tag{3}$$

κ and u_* represent the Von Karman constant and the bottom shear velocity. $\sigma = z/h$ is the adimensionalized height.

$$\frac{\overline{c}}{c^a} = \left(\frac{1 - \sigma}{\sigma} \frac{\sigma^a}{1 - \sigma^a} \right)^{\frac{w_s}{\kappa u_*}} \tag{4}$$

[1] Laboratoire de Morphodynamique Continentale et Côtière, UMR6143, Université de Caen, Caen, France.
[2] LUSAC, EA 2607, Ecole d'Ingénieurs de Cherbourg, Université de Caen, Octeville, France.

0148-0227/08/2007JC004708

[5] The classical sediment transport models are based on similar considerations, the passive scalar hypothesis is assumed in which the fields of fluid velocity and pressure are determined without considering the influence of sediment particles. A mass balance is solved to calculate the sediment concentration by assuming no interaction between sediment particles and fluid flow. This implies that the horizontal velocity of sediments is equal to that of the fluid. The sediment vertical velocity differs from that of the fluid because of a settling velocity that accounts for the difference in the true density between sediment particles and the surrounding fluid. The particle's turbulent vertical flux is modeled following *Rouse*'s [1937] concept in the mass balance equation. The turbulent sediment diffusivity is usually modeled using an empirical relation between the fluid eddy viscosity and the sediment turbulent diffusivity [*Van Rijn*, 1984]. The influence of sediment particles on fluid flow turbulence is either neglected [*Duy and Shibayama*, 1997] or incorporated as a dissipative term in the turbulent kinetic energy transport equation based on an analogy with density stratification [*Smith and McLean*, 1977; *Vilaret and Davies*, 1995].

[6] All the hypotheses mentioned above are very restrictive and not always verified. Experimental work carried out by *Kaftori et al.* [1996], *Muste and Patel* [1997], *Muste et al.* [2005], amongst others, has shown the existence of a horizontal velocity difference between sediment particles and the fluid especially for sufficiently massive particles such as sand. This is in contradiction to one of the hypotheses assumed in the classical approach for sediment transport modeling. *Muste et al.* [2005] observed that turbulent intensities are damped or enhanced depending on particle inertia and on the distance from the bed. This cannot be represented by the analogy with density stratification that always must be a damping term. Moreover, the dispersion effects of particles by the fluid turbulent motion based on *Rouse* [1937] concept is not correct for massive particles (i.e., Stokes number St $\gg 1$ with $St = \tau_{fs}/\tau_f$ where τ_{fs} is the particle relaxation time and τ_f is a time scale of the fluid flow). In fact, the diffusion coefficient of large particles is greater than the fluid's eddy viscosity [*Coleman*, 1970]. While there is no theory developed to cover this aspect a calibration of the sediment's diffusivity is needed to represent correctly the sediment particle concentration profile. All these comments show the limitations of the classical model.

[7] The two-phase flow modeling approach gives a theoretical framework to describe the physical processes more accurately than in the classical model by reducing the latter models restrictive assumptions.

[8] Two-phase flow models have been developed since the 1970s for application in the field of chemical and mechanical engineering [*Ishii*, 1975; *Drew and Lahey*, 1993; *Gidaspow*, 1994; *Enwald et al.*, 1996]. Two-phase flow equations have also been applied to sediment transport problems [*Drew*, 1983; *Vilaret and Davies*, 1995; *Greimann et al.*, 1999; *Barbry et al.*, 2000; *Greimann and Holly*, 2001; *Hsu et al.*, 2003; *Amoudry et al.*, 2005]. In this approach, the medium is decomposed into two phases: a fluid phase (water) and a solid or particulate phase (sediment particles). Conservation equations for mass and momentum are derived for both phases by applying an averaging procedure to the local instantaneous conservation equations. The averaging operator can be either time or space or both depending on the nature of the problem. The statistical treatment used to derive the model's equations introduces interfacial momentum terms, stress tensors and turbulent correlations that must be modeled. Interactions between sediment particles and the fluid are accounted for in the governing equations by the presence of transfer terms of mass, momentum and energy. Two classes of two-phase flow models exist to solve the set of partial differential equations: the mixed flow model where a momentum equation for the mixture is obtained by combining momentum equations for each phase and the two-fluid model where momentum equations are solved separately for each of the phases. This last class of model is the most general one because velocity fields for both phases are distinguished and there is no assumption concerning the equality of horizontal velocity between fluid and sediment particles. The fundamental difference between the two-phase flow model and the classical approach concerns the vertical velocity. In the classical approach, the vertical velocity is simply the sediment particle settling velocity whereas in the two-phase flow approach, this velocity is obtained by solving the vertical momentum equation for the solid phase.

[9] Recently, *Greimann et al.* [1999] have applied two-phase flow equations to a steady, uniform open channel flow and derived analytical solutions for sediment transport. These authors have focused their attention on the effects of fluid turbulence on the behavior of suspended particles. Following *Simonin* [1991] the dispersion of particles by the fluid turbulent motion is modeled by a drift velocity appearing in the relative velocity expression. The dispersion coefficient is related to the correlation between the fluctuating fluid and particles velocities multiplied by the time that a particle spends in the fluid eddy. The damping of turbulence is represented in the model by decreasing the Von Karman constant in agreement with experimental measurements. They derived an analytical solution for the concentration profile in dilute flow conditions and for the horizontal velocity difference between sediment particles and the fluid, called lag velocity (see details in Appendix C). *Greimann et al.* [1999] give a theoretical justification for the modification of the *Rouse* [1937] exponent (Z_R) to represent the increased diffusive flux of large particles which is due to vertical turbulent stress of the solid phase. According to the authors dimensional analysis this term increases with particles inertia for given flow conditions. Experimental investigations of *Sumer and Deigaard* [1981] and *Rashidi et al.* [1990], amongst others, have shown that particles suspended in a turbulent flow are correlated with the area of positive vertical velocity fluctuations of the fluid. If not, particles would sink to the bed and never be resuspended. Because of the negative value of the Reynolds stress $\langle u_f' w_f' \rangle_f$, it follows that particles are also correlated with area of negative horizontal velocity fluctuations of the fluid. This physical interpretation shows that horizontal velocity of particles is lower than the horizontal velocity of the fluid. The analytical solution proposed by *Greimann et al.* [1999] represents this feature of the flow. *Greimann and Holly* [2001] extended their work and presented a semianalytical solution for the concentration profile by including particle-particle interactions based on the kinetic theory of granular

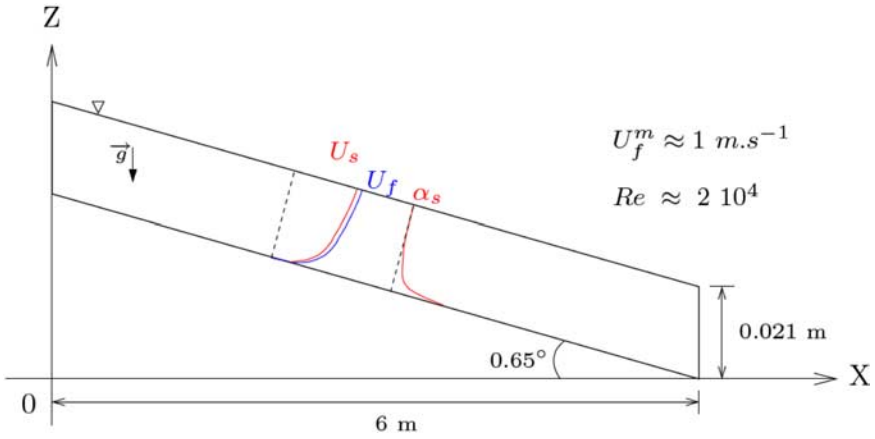

Figure 1. Experimental configuration of *Muste et al.* [2005].

flows [*Chapman and Cowling*, 1970]. This new solution improves upon the original analytical solution when sediment particles concentration in volume is of the order of 0.1.

[10] More recently, *Hsu et al.* [2003] have presented a two-phase flow model based on the original equations of *Drew* [1983]. A *Favre* [1965] averaging technique is applied to the original two-phase equations to account for the large-scale turbulence. This technique introduced extra terms into the momentum conservation equation: a large-scale Reynolds stress and the correlation between the concentration fluctuations and the fluid velocity fluctuations. This last term represents the turbulent sediment vertical flux induced by the large-scale fluid turbulent motion. The authors used the closure proposed by *Drew* [1976] and *Ma and Ahmadi* [1988] for the dissipation term in the fluid turbulent kinetic energy equation. This closure is based on the assumption that the cross correlation of the velocity fluctuations for the fluid and the particles can be related to the fluid velocity correlation by the ratio $\frac{\tau_f^t}{\tau_f^t+\tau_{fs}}$ where τ_f^t is the fluid turbulence time scale and τ_{fs} is the particle relaxation time. The models equations are solved in two ways: a semianalytical approach and a numerical approach. The numerical solution is tested against experimental data and is used to check the validity of boundary approximations made in the semianalytical approach. *Amoudry et al.* [2005] have used the same numerical model but applied to a pure oscillatory flow and an oscillatory flow superimposed on a mean current. Authors have investigated a concentration-dependent Schmidt number and two near-bed boundary conditions: an empirical pickup function and a reference concentration. Using a concentration-dependent Schmidt number, results obtained with the reference concentration boundary condition are an improvement upon the pickup function approach.

[11] *Muste et al.* [2005], on the basis of the experiments of *Raudkivi* [1998], amongst others, show that the mixed fluid or classical approach for sediment transport is of limited validity and that more research should be oriented toward understanding and formulating the actual physical processes involved in sediment transport. In their own results *Muste et al.* [2005] conclude that the mixed fluid approach admits some inconsistencies especially concerning the way energy transfer between the fluid and the particles are represented in this type of model. In the same way *Hsu et al.* [2003] argued, on the basis of experimental work of *Gore and Crowe* [1989] and *Hetsroni* [1989], that an appropriate turbulence model describing fluid particle flow should be able to represent a damping or an enhancement of the fluid turbulent kinetic energy depending upon the particle characteristics and the flow conditions.

[12] In the present paper, we propose to apply a 2-D vertical two-phase flow model (K. Nguyen et al., A two-phase numerical model for suspended-sediment transport in estuaries, submitted to *Advances in Water Resources*, 2008) to a steady, uniform sediment-laden flow in an open channel. Different turbulence models taken from the literature on fluidized beds are implemented and tested. The main objective of this paper is to propose an appropriate set of two-phase equations with pertinent closures. We focus our attention more especially on the modeling of the fluid particle turbulent interactions in terms of dispersion of particles by the fluid turbulent motion and the transfer of turbulent kinetic energy between the fluid and the particles. In order to discuss the appropriateness of turbulence closures we compare numerical results with experimental data from *Muste et al.* [2005]. We consider a two-dimensional, unidirectional, free surface flow, driven by gravity in an inclined channel with a small inclination angle (see Figure 1). Two different types of particles have been used: crushed nylon particles and natural sand particles.

[13] The theoretical formulation of the two-phase flow model is presented in section 2 including the description of four turbulence models of increasing complexity. We have restricted the turbulence modeling to the first-order approximation. The dispersion effect due to particle transport by turbulent fluid motion is modeled by a drifting velocity appearing in the interfacial momentum transfer term [*Simonin*, 1991]. In section 3, an overview of the numerical methods used in the model is proposed. The experimental setup and the numerical settings, including boundary conditions, are detailed in section 4. In section 5 the numerical results are compared with the experimental data of *Muste et al.* [2005] and analytical solutions of *Rouse* [1937] and *Greimann et al.* [1999] for the lag velocity and the sediment concentration profile for the two types of particles. In section 6, we shall attempt to discuss the turbulent closures

used in the two-phase flow model for sediment transport and the improvement of the two-phase flow model upon the classical model of sediment transport.

2. Theoretical Formulation

2.1. Governing Equations

[14] The present model is based on averaged balance equations for each phase, fluid and sediment [*Barbry et al.*, 2000; *Barbry*, 2000]. The local instantaneous equations are averaged by an ensemble average operator and a weighting procedure is applied to the variables [*Drew and Lahey*, 1993; *Drew*, 2001]. Using this procedure averaged balance equations for mass (5) and momentum (6) are derived:

$$\frac{\partial \alpha_k \langle \rho_k \rangle_k}{\partial t} + \overrightarrow{\nabla}.\left(\alpha_k \langle \rho_k \rangle_k \langle \overrightarrow{u_k} \rangle_k\right) = \frac{D\alpha_k \langle \rho_k \rangle_k}{Dt} = 0 \tag{5}$$

$$\frac{D\alpha_k \langle \rho_k \rangle_k \langle \overrightarrow{u_k} \rangle_k}{Dt} = \overrightarrow{\nabla}.\left[\alpha_k \left(\left\langle \overline{\overline{T_k}} \right\rangle_k + \overline{\overline{T_k^{Re}}}\right)\right] + \alpha_k \langle \rho_k \rangle_k \overrightarrow{g} - \overrightarrow{M_k} \tag{6}$$

[15] The average operator $\langle \cdot \rangle_k$ represent either a phase average or a mass average [*Favre*, 1965]. α_k, $\langle \overrightarrow{u_k} \rangle_k$, $\langle \rho_k \rangle_k$ are the volume fraction, mean velocity vector and mean density of phase k. $\overrightarrow{g}$ is the acceleration of gravity. $\left\langle \overline{\overline{T_k}} \right\rangle_k$ and $\overline{\overline{T_k^{Re}}} = -\rho_k \langle \overrightarrow{u_k'} \otimes \overrightarrow{u_k'} \rangle_k$ represents the viscous stress tensor and the Reynolds stress tensor, respectively. $\overrightarrow{M_k}$ is the interfacial momentum transfer between fluid and solid phases.

[16] The averaging procedure applied to the local instantaneous equations introduces more unknowns than the number of equations. Therefore, additional expressions are needed to close the set of equations as turbulent correlations, stress tensor and interfacial momentum transfer between phases [*Enwald et al.*, 1996; *Peirano and Leckner*, 1998].

[17] We point out that the volume conservation imposes:

$$\alpha_f + \alpha_s = 1 \tag{7}$$

[18] For sake of clarity, we have omitted the ensemble average operator, $\langle \rangle_k$, when there was no ambiguity.

2.2. Closures for Sediment Particle Equations

2.2.1. Interfacial Momentum Transfer

[19] The interfacial momentum transfer term $\overrightarrow{M_k}$ arises from stresses acting on the interface. It is defined following *Drew and Lahey* [1993] by equation (8).

$$\overrightarrow{M_k} = p_{ki} \overrightarrow{\nabla} \alpha_k - \overline{\overline{\tau}}_{ki} \overrightarrow{\nabla} \alpha_k + \overrightarrow{M_k'} \tag{8}$$

[20] The first two terms represent the interfacially averaged pressure p_{ki} and shear stress $\overline{\overline{\tau_{ki}}}$ of phase k. And the last term $\overrightarrow{M_k'}$ represents forces associated with drag, virtual mass, lift forces and unsteady effects. In the case of small sediment particles, such as sand (*diameter* $\approx$ 200 μm), falling under the effect of gravity the particulate Reynolds number $Re_p = \frac{\alpha_f d \| \overrightarrow{u_r} \|}{\nu_f}$ [*Drew and Lahey*, 1993] is of order unity and so the drag force is dominant [*Hsu et al.*, 2003]. In a first approach we only consider the drag force in the interfacial momentum transfer term. The drag force is written in terms of the mean relative velocity $\overrightarrow{u_r}$ and the particle relaxation time τ_{fs}.

$$\overrightarrow{M_s'} = -\overrightarrow{M_f'} = \frac{1}{\tau_{fs}} \alpha_s \rho_s \overrightarrow{u_r} \tag{9}$$

[21] The mean relative velocity is defined by (10)

$$\overrightarrow{u_r} = \overrightarrow{u_s} - \overrightarrow{u_f} - \overrightarrow{u_d} \tag{10}$$

where $\overrightarrow{u_d} = \langle \overrightarrow{u_f'} \rangle_s$ represents the correlation between the fluctuating velocity of the fluid phase and the spatial distribution of the solid phase. This term, called the drift velocity, represents the dispersion of particles by the large scale of the fluctuation motion in the fluid phase, large with respect to the particle diameter [*Simonin and Viollet*, 1990].

[22] The particle relaxation time is defined by [*Enwald et al.*, 1996]:

$$\tau_{fs} = \frac{4 d \rho_s}{3 \rho_f C_D \| \overrightarrow{u_r} \|} \alpha_f^{-2.65} \tag{11}$$

where C_D is the averaged drag coefficient for a single particle in a suspension. It is given by the equation [*Haider and Levenspiel*, 1989]:

$$C_D = \frac{24}{Re_p}\left(1 + c_1 {Re_p}^{c_2}\right) + \frac{c_3}{1 + c_4/Re_p} \tag{12}$$

$$\begin{aligned} c_1 &= e^{2.33 - 6.49\psi + 2.45\psi^2} \\ c_2 &= 0.10 + 0.56\psi \\ c_3 &= e^{4.91 - 13.90\psi + 18.42\psi^2 - 10.26\psi^3} \\ c_4 &= e^{1.47 + 12.26\psi - 20.73\psi^2 + 15.89\psi^3} \end{aligned} \tag{13}$$

where Re_p is the mean particle Reynolds number defined by $Re_p = \frac{\alpha_f d \| \overrightarrow{u_r} \|}{\nu_f}$ [*Drew and Lahey*, 1993]. The shape factor $\psi = A_s/A_p$ takes into account the form of the particle. It is defined by the ratio of the surface area of the equivalent spherical particle of diameter d (A_s) and the real surface area of the particle (A_p). The shape factor is always less than unity meaning that non spherical particles have a larger surface area than spherical ones. Consequently, the drag coefficient increases with increasing deviation from spherical shape.

[23] A model for the drift velocity, proposed by *Deutsch and Simonin* [1991], is expressed as:

$$\overrightarrow{u_d} = \overline{\overline{D_{fs}^t}} \left(\frac{\overrightarrow{\nabla} \alpha_f}{\alpha_f} - \frac{\overrightarrow{\nabla} \alpha_s}{\alpha_s} \right) \tag{14}$$

[24] On the basis of semiempirical analysis, the dispersion tensor is expressed in terms of the covariance between the turbulent velocity fluctuations of the two phases and a fluid particle turbulent time component:

$$\overline{\overline{D_{fs}^t}} = \tau_{fs}^t \left\langle \overrightarrow{u_f'} \otimes \overrightarrow{u_s'} \right\rangle_s \tag{15}$$

$$\tau_{fs}^{t} = \gamma_s \tau_f^{t} \quad with \quad \gamma_s = \left[1 + C_\beta \cdot \sqrt{\left(3 \parallel \overrightarrow{u_r} \parallel^2\right)/\left(2k_f\right)}\right]^{-1/2} \tag{16}$$

[25] The fluid particle turbulent time scale can be written following *Csanady* [1963] as given by equation (16). It is mainly related to the loss of correlation between the turbulent motions of the fluid and particles due to the mean relative motion of the particles (''crossing-trajectories effects''). The value of the coefficient C_β depend on the direction of the flow, $C_\beta = 0.45$ in the direction orthogonal to the mean relative velocity and $C_\beta = 1.8$ in the direction parallel to the mean relative velocity. These values were determined by *Deutsch and Simonin* [1991] on the basis of experimental data of *Wells and Stock* [1983].

[26] *Drew* [2001] proposed a similar model for the turbulent dispersion of particles or bubbles. The two-phase flow model is derived on the basis of a Boltzmann equation. The dispersion is the result of the correlation between the fluid velocity with the trajectories of individual particles. The dispersion ''force'' derived by the author is equal to the scalar product of the Reynolds stress tensor for the solid phase with the gradient of the solid phase volume fraction. The dispersion tensor depends on the ratio of the particle relaxation time to the fluid turbulence time scale. This model is similar to Simonin's model. The main difference concerns the use of the solid phase Reynolds stress tensor in the dispersion term by *Drew* [2001] whereas *Simonin and Viollet* [1990] used the covariance between the turbulent velocity fluctuations of the two phases. This difference is due to the assumption that particles did not affect the fluid turbulence in Drew's model.

2.2.2. Constitutive Law

[27] Concerning the constitutive assumptions, we have used the general expression for the stress tensor given by *Drew and Lahey* [1993] with the closure proposed by *Lundgren* [1972] for the effective viscosity (17).

$$\begin{cases} \alpha_f \overline{\overline{\tau_f}} = \alpha_f 2\mu_f \overline{\overline{D_f}} + \alpha_s 2\mu_f \overline{\overline{D_s}} \\ \alpha_s \overline{\overline{\tau_s}} = \alpha_s \alpha_f \beta 2\mu_f \overline{\overline{D_f}} + \alpha_s^2 \beta 2\mu_f \overline{\overline{D_s}} \end{cases} \tag{17}$$

$\overline{\overline{D_k}}$ represent the mean strain rate tensor of phase k:

$$\overline{\overline{D_k}} = \frac{1}{2}\left(\overrightarrow{\nabla}\overrightarrow{u_k} + \left(\overrightarrow{\nabla}\overrightarrow{u_k}\right)^T\right) \tag{18}$$

[28] An amplification factor for the viscosity, β, accounts for the non-Newtonian characteristics of the flow when the volume fraction of the solid phase reaches high values. We have use the formulation of *Graham* [1981]. This formulation is consistent with the expression proposed by *Einstein* [1906] in the dilute case and with the expression proposed by *Frankel and Acrivos* [1967] for dense suspension.

$$\beta = \frac{5}{2} + \frac{9}{4}\frac{\alpha_s}{1 + d_{ip}/d} \left(\frac{1}{2d_{ip}/d} - \frac{1}{1 + 2d_{ip}/d} - \frac{1}{\left(1 + 2d_{ip}/d\right)^2}\right) \tag{19}$$

d_{ip} is the interparticle spacing and d the particle diameter. *Drew and Lahey* [1993] proposed the following formulae to express the ratio of the interparticular spacing to the particle diameter:

$$\frac{d_{ip}}{d} = \frac{1 - \left(\alpha_s/\alpha_s^{\max}\right)^{1/3}}{\left(\alpha_s/\alpha_s^{\max}\right)^{1/3}}$$

where $\alpha_s^{\max}$ is the solid volume fraction for maximum packing of spheres. For a simple cubic packing of rigid spheres $\alpha_s^{\max} = 0.625$.

[29] The viscous stress for the sediment phase represents the modification of the rheology of the suspension due to the presence of particles. Assuming that the shear rate for both phases is equal, i.e., $\overline{\overline{D_f}} = \overline{\overline{D_s}}$ the viscous stress of the mixture can be recovered from equation (17):

$$\begin{aligned} \overline{\overline{\tau_{mix}}} &= \alpha_f \overline{\overline{\tau_f}} + \alpha_s \overline{\overline{\tau_s}} \\ \overline{\overline{\tau_{mix}}} &= 2\left[\underbrace{\left(\alpha_s + \alpha_f\right)}_{=1}\alpha_s \beta \mu_f + \mu_f\right]\overline{\overline{D_f}} \\ \overline{\overline{\tau_{mix}}} &= 2\mu_f(1 + \alpha_s\beta)\overline{\overline{D_f}} \end{aligned}$$

2.2.3. Turbulence Modeling

[30] Four turbulence models are introduced in the two-phase flow model [*Chauchat*, 2007]. For sake of simplicity they will be denoted T1, T2, T3 and T4 hereafter. The fluid phase turbulence is always modeled using a $k - \varepsilon$ type model based on *Simonin and Viollet* [1990]. The first two models, T1 and T2, do not simulate either the solid phase turbulence or the fluid-solid turbulent interactions. In the first one (T1), the dispersion is not represented whilst in the second one (T2) the dispersion is modeled using an approximation explained later. The two last models, T3 and T4, solve the solid phase turbulence and the fluid-solid turbulent interactions. In the model T3, the turbulent kinetic energy for the solid phase (k_s) and the fluid particle covariance (k_{fs}) are related to the turbulent kinetic energy for the fluid phase (k_f) by algebraic equations [*Simonin*, 1991]. Finally, the model T4 solves 2 transport equations for the turbulent kinetic energy for the solid phase (k_s) and the fluid particle covariance (k_{fs}) [*Boëlle et al.*, 1994]. This model is based on the kinetic theory of granular flows [*Jenkins and Richman*, 1985].

[31] These two-phase flow turbulence models were originally developed for gas-solid mixtures. *Vilaret and Davies* [1995], *Greimann et al.* [1999], *Greimann and Holly* [2001], amongst others, applied these models to sediment transport modeling, i.e., liquid-solid mixture problems. In this work, we also use turbulence closures developed for gas-solid mixtures.

[32] A summary of the four turbulence models implemented in the numerical model is presented in Table 1.

2.2.3.1. Turbulence Model for Fluid Phase

[33] The fluid turbulence modeling is based on the model proposed by *Simonin and Viollet* [1990]. This is a $k - \varepsilon$ type model modified to take into account the influence of suspended particles. Additional terms are included to account for turbulent momentum transfer between phases.

Table 1. Summary of Turbulence Models Implemented in the Numerical Model

Notations	Fluid Phase Turbulence	Solid Phase Turbulence	Dispersion $\overline{\overline{D_{fs}^t}}$
T1	k_f–ε_f model	–	0
T2	k_f–ε_f model	–	${\tau_{fs}}^t \langle \overrightarrow{u_f'} \otimes \overrightarrow{u_f'} \rangle$
T3	k_f–ε_f model	algebraic model	${\tau_{fs}}^t \langle \overrightarrow{u_f'} \otimes \overrightarrow{u_s'} \rangle$
T4	k_f–ε_f model	k_s–k_{fs} model	${\tau_{fs}}^t \langle \overrightarrow{u_f'} \otimes \overrightarrow{u_s'} \rangle$

[34] Equations for the turbulent kinetic energy and dissipation rate of turbulent kinetic energy of the fluid phase are written as follows:

$$\frac{D\alpha_f \rho_f k_f}{Dt} = \overrightarrow{\nabla} \cdot \left(\alpha_f \left(\mu_f + \frac{\mu_f^t}{\sigma_k} \right) \overrightarrow{\nabla} k_f \right) - \alpha_f \rho_f \epsilon_f - \alpha_f \rho_f \{ \left\langle \vec{u_f'} \otimes \vec{u_f'} \right\rangle_f \overrightarrow{\nabla} \}^T \vec{u_f} + \Pi_{k_f} \tag{20}$$

$$\frac{D\alpha_f \rho_f \epsilon_f}{Dt} = \overrightarrow{\nabla} \cdot \left(\alpha_f \left(\mu_f + \frac{\mu_f^t}{\sigma_\epsilon} \right) \overrightarrow{\nabla} \epsilon_f \right) + \Pi_{\epsilon_f} - \alpha_f \rho_f \frac{\epsilon_f}{k_f} \left(C_{\epsilon_1} \{ \left\langle \overrightarrow{u_f'} \otimes \vec{u_f'} \right\rangle_f \overrightarrow{\nabla} \}^T \vec{u_f} + C_{\epsilon_2} \epsilon_f \right) \tag{21}$$

[35] The Reynolds stress tensor of the fluid phase $\overline{\overline{T_f^{Re}}}$ is modeled using the Boussinesq model [*Peirano and Leckner*, 1998].

$$\overline{\overline{T_f^{Re}}} = -\frac{2}{3} \rho_f k_f \overline{\overline{I}} + 2\rho_f \nu_f^t \left[\overline{\overline{D_f}} - \frac{1}{3} (\nabla \overrightarrow{u_f}) \overline{\overline{I}} \right] \tag{22}$$

[36] The kinematic turbulent viscosity of the fluid phase, ν_f^t is defined by $\nu_f^t = 2\, k_f\, \tau_f^t/3$, and the time scale of the large eddies by $\tau_f^t = \frac{3}{2}\, C_\mu\, k_f/\varepsilon_f$ [*Simonin*, 1991].

[37] In the equations (20) and (21) the terms $\Pi_{k_f \text{ and } \Pi\varepsilon_f}$ represent the interaction terms, they are defined as follows:

$$\Pi_{k_f} = \frac{\alpha_f \rho_f}{\tau_{fs}} \left(-2k_f + k_{fs} + \overrightarrow{u_d} \cdot \overrightarrow{u_r} \right) \tag{23}$$

$$\Pi_{\epsilon_f} = C_{\epsilon_3} \frac{\epsilon_f}{k_f} \Pi_{k_f} \tag{24}$$

[38] The interaction term for the fluid turbulent kinetic energy (equation (23)) can be split into two contributions. The first one is $\frac{\alpha_f \rho_f}{\tau_{fs}}$ $(-2\ k_f + k_{fs})$. This term leads to the destruction or the production of the fluid turbulence according to the value of the fluid particle velocity covariance k_{fs} with regard to the fluid turbulent kinetic energy. The second contribution is $\frac{\alpha_f \rho_f}{\tau_{fs}} \overrightarrow{u_d}.\overrightarrow{u_r}$ which corresponds to the Work of the drag force associated with the fluid turbulent motion. This term is a damping term if $\overrightarrow{u_d}$ and $\overrightarrow{u_r}$ are in opposite direction.

[39] The values used in the $k_f - \varepsilon_f$ model are chosen as $C_\mu = 0.09$, $C_\varepsilon 1 = 1.44$, $C_{\varepsilon 2} = 1.92$, $C_{\varepsilon 3} = 1.2$, $\sigma_k = 1$ and $\sigma_\varepsilon = 1.2$. All these constants have standard single phase values except $C_{\varepsilon 3}$. This constant is included in the interaction terms for dissipation and has been determined empirically from turbulent gas particle jet flows [*Elghobashi and Abou-Arab*, 1983].

[40] The bottom boundary layer cannot be treated directly by the $k - \varepsilon$ model. Different solutions exist [*Mohammadi and Pironneau*, 1994]. The easiest one is to set the computational domain above the viscous sublayer, in the logarithmic region, then to impose the value of the stream-wise velocity and the fluid phase kinetic energy from the logarithmic law of the wall. Another solution consists of introducing functions depending on the Reynolds number that modify the coefficients of the standard $k - \varepsilon$ model in the near-wall region. This is the so-called "Low Reynolds number $k - \varepsilon$" model. Because of very strong vertical gradient, the mesh has to be very fine in the near wall region. A third solution, is found in the $k - \varepsilon$ two-layer model [*Mohammadi and Pironneau*, 1994] this technique is more robust and stable than the "Low Reynolds number $k - \varepsilon$" model and, especially, does not require a so fine mesh near the wall. We chose this late technique for the numerical model (see Appendix A for details).

[41] The effect of the presence of particles in the low Reynolds number layer is represented in the model by the transfer term (Π_{kf}) in the turbulent kinetic energy transport equation (20). This term also represents the feedback of the presence of the particles on the dissipation rate of the turbulent kinetic energy and the eddy viscosity in the low Reynolds number layer. Thus, the expressions for these two quantities are proportional to the turbulent kinetic energy at a given exponent.

[42] It should be noted that the T1 model hypothesis implies that the turbulence interaction between the fluid and solid phase and the dispersion of particles by the fluid turbulent motion are neglected. So, interaction terms Π_{k_f} and Π_{ε_f} in the transport equations (20) and (21) are set to zero. Also, the dispersion tensor in the drift velocity definition (14) is null.

$$\begin{aligned} \Pi_{k_f} = \Pi_{\epsilon_f} = 0 \\ \overline{\overline{D_{fs}^t}} = 0 \end{aligned} \tag{25}$$

[43] The Reynolds stress tensor for the solid phase is set equal to the fluid one (i.e., $\overline{\overline{T_s^{Re}}} = \overline{\overline{T_f^{Re}}}$).

[44] For the T2 turbulence model it should be noted that we assumed that the covariance of the fluctuating velocities of both phases is equal to the covariance of the fluid fluctuating velocities: $\left\langle \overrightarrow{u_f'} \otimes \overrightarrow{u_s'} \right\rangle_s = \left\langle \overrightarrow{u_f'} \otimes \overrightarrow{u_f'} \right\rangle_f$. This assumption has been used by *Greimann et al.* [1999], as pointed out by the authors it may overestimate the fluid-sediment correlations because the sediment does not follow, exactly, the fluid turbulent motion due to their relative motion.

[45] The consequences of this assumption on the model's equations are a simplification of the interaction terms:

$$\Pi_{k_f} = \frac{\alpha_f \rho_f}{\tau_{fs}} \left(\underbrace{-2k_f + k_{fs}}_{=0} + \overrightarrow{u_d} \cdot \overrightarrow{u_r} \right),$$

and of the dispersion tensor:

$$\overline{\overline{D_{fs}^t}} = \tau_{fs}^t \left\langle \overrightarrow{u_f'} \otimes \overrightarrow{u_f'} \right\rangle_f .$$

[46] This model is the most similar in its assumptions, regarding the other presented models, to the classical approach.

2.2.3.2. Turbulence Models for Solid Phase: The $k_s - k_{fs}$ Model

[47] The turbulence model for the solid phase originates from the framework of the kinetic theory of granular flow [*Jenkins and Richman*, 1985]. The k_s - k_{fs} model is based on two transport equations, one for the turbulent kinetic energy of the solid phase, k_s (26), and one for the fluid particle velocity covariance, k_{fs} (30) [*Simonin*, 1991].

$$\frac{D\alpha_s\rho_s k_s}{Dt} = \overrightarrow{\nabla} \cdot \left(D_{ks} \overrightarrow{\nabla} k_s \right) - \alpha_s \rho_s \frac{1-e^2}{3\tau_s^c} k_s - \alpha_s \rho_s \{ \left\langle \overrightarrow{u_s'} \otimes \overrightarrow{u_s'} \right\rangle_s \overrightarrow{\nabla} \}^T \overrightarrow{u_s} + \Pi_{ks} \tag{26}$$

where $D_{ks} = \alpha_s \rho_s (K_s^t + K_s^c)$, K_s^t and K_s^c represent the turbulent and collisional diffusivity. There expressions are given in Appendix B.

[48] Therefore, the Reynolds stress tensor for the solid phase $\overline{\overline{T_s^{Re}}}$ can be expressed following the Boussinesq model (27) [*Simonin*, 1991].

$$\overline{\overline{T_s^{Re}}} = -\frac{2}{3}\rho_s k_s \overline{\overline{I}} + 2\rho_s \nu_s^t \left[\overline{\overline{D_s}} - \frac{1}{3} \left(\nabla \overrightarrow{u_s} \right) \overline{\overline{I}} \right] \tag{27}$$

where the solid phase turbulent viscosity is given by (28):

$$\nu_s^t = \left[\nu_{fs}^t + \frac{1}{3}\tau_{fs} k_s \right] \left[1 + \frac{\sigma_s \tau_{fs}}{2\tau_s^c} \right]^{-1} \tag{28}$$

[49] In equation (26), the term Π_{ks} represent the interaction with fluid turbulent motion.

$$\Pi_{ks} = -\frac{\alpha_s \rho_s}{\tau_{fs}} \left(2k_s - k_{fs} \right) \tag{29}$$

[50] The fluid particle velocity covariance, k_{fs}, is defined as the trace of the tensor $\left\langle \overrightarrow{u_f'} \otimes \overrightarrow{u_s'} \right\rangle$. A transport equation is obtained, in a similar manner to the Reynolds stress tensor equation in the single phase case, by averaging the Navier-Stokes operator for the fluid phase (6) multiplied by the fluctuating part of the solid phase velocity plus the Navier-Stokes operator for the solid phase multiplied by the fluctuating part of the fluid phase velocity. Some higher-order terms appear in this equation that have to be closed. The resulting equation is presented here (30) [*Simonin*, 1991]:

$$\frac{D\alpha_s\rho_s k_{fs}}{Dt} = \overrightarrow{\nabla} \cdot \left(\alpha_s \rho_s \frac{\nu_{fs}^t}{\sigma_{k_s}} \overrightarrow{\nabla} k_{fs} \right) - \alpha_s \rho_s \epsilon_{fs} - \alpha_s \rho_s \{ \left\langle \vec{u}_f' \otimes \vec{u}_s' \right\rangle_s \overrightarrow{\nabla} \}^T \vec{u}_s - \alpha_s \rho_s \{ \left\langle \vec{u}_s' \otimes \vec{u}_f' \right\rangle_s \overrightarrow{\nabla} \}^T \vec{u}_f + \Pi_{kfs} \tag{30}$$

[51] The fluid particle velocity covariance $\left\langle \overrightarrow{u_f'} \otimes \overrightarrow{u_s'} \right\rangle_s$ tensor is obtained by a Boussinesq model [*Peirano and Leckner*, 1998]:

$$\left\langle \overrightarrow{u_f'} \otimes \overrightarrow{u_s'} \right\rangle_s = -\frac{1}{3} k_{fs} \overline{\overline{I}} + \nu_{fs}^t \left[\overline{\overline{D_{fs}}} - \frac{1}{3} Tr\left(\overline{\overline{D_{fs}}} \right) \overline{\overline{I}} \right] \tag{31}$$

where $\overline{\overline{D_{fs}}} = \overrightarrow{\nabla} \overrightarrow{u_f} + \left(\overrightarrow{\nabla} \overrightarrow{u_s} \right)^T$ is the strain rate tensor. The turbulent fluid particle viscosity is given by $\nu_{fs}^t = \frac{k_{fs}\tau_{fs}^t}{3}$. The two following terms correspond to the production of fluid particle velocity covariance by the mean flow.

[52] The dissipation, ϵ_{fs}, is given by $\epsilon_{fs} = k_{fs}/\tau_{fs}^t$ and is a function of the fluid particle velocity covariance k_{fs} and the eddy interaction time τ_{fs}^t. Meaning that the destruction of covariance is due to viscous effects in the fluid phase and crossing-trajectories effects.

[53] Finally, the interaction term, Π_{kfs}, is expressed by (32) with $X_{fs} = \frac{\alpha_s \rho_s}{\alpha_f \rho_f}$

$$\Pi_{kfs} = -\frac{\alpha_s \rho_s}{\tau_{fs}} \left(\left(1 + X_{fs} \right) k_{fs} - 2X_{fs} k_s - 2k_f \right) \tag{32}$$

2.2.3.3. Turbulence Models for Solid Phase: Algebraic Model

[54] In the case of dilute dispersion of heavy particles in a homogeneous, isotropic and steady turbulent fluid flow *Tchen* [1947] derived the following equations for the particle correlation and the fluid particle correlation functions using an exponential form for the fluid turbulence Lagrangian function:

$$\left\langle \overrightarrow{u_s'} \otimes \overrightarrow{u_s'} \right\rangle_s = \left\langle \overrightarrow{u_f'} \otimes \overrightarrow{u_f'} \right\rangle_s \frac{b^2 + \xi}{1 + \xi} \tag{33}$$

and

$$\left\langle \overrightarrow{u_f'} \otimes \overrightarrow{u_s'} \right\rangle_s = \left\langle \overrightarrow{u_f'} \otimes \overrightarrow{u_f'} \right\rangle_s \frac{b + \xi}{1 + \xi}, \tag{34}$$

with $b = \rho_f/\rho_s$ and $\xi = \tau_{fs}^t/\tau_{fs}$.

[55] *Simonin* [1991] derived similar equations from asymptotic analysis of the two-phase flow equations.

[56] The correlation functions are computed using the eddy viscosity concept as in the k_s - k_{fs} model (27) and (31). From equation (28), the particulate viscosity can be written as:

$$\nu_s^t = \nu_{fs}^t + \frac{1}{2}\tau_{fs} \frac{2}{3} k_s \tag{35}$$

and the fluid particle turbulent viscosity is written:

$$\nu_{fs}^t = \frac{\tau_{fs}^t k_{fs}}{3}, \tag{36}$$

as in the $k_s - k_{fs}$ model.

3. Numerical Methods

[57] The complete set of equations (5), (6), (20) and (21) plus equations (26) and (30) for the T4 turbulence model are solved by a fractional step procedure that is briefly described as follows. A projection method of *Chorin* [1968] and *Temam* [1969] is used to solve the coupled set of

Table 2. Sediments Characteristics

	NS: Natural Sand	NBS: Crushed Nylon
d_p (μm)	230 ± 20	230 ± 20
ρ_s (kg m^{-3})	2650	1025 ± 5
W_{fal} (m s^{-1})	0.024	0.0006
τ_{fs} (s)	0.0052	0.0029

equations formed [*Guillou et al.*, 2000]. In order to avoid spurious oscillations that could be produced by the projection method [*Guillou and Nguyen*, 1999] a staggered grid is used [*Harlow and Welch*, 1965]. The finite difference technique is used for the discretization of the equations except for the mass conservation equation for the solid phase (5). Indeed this equation is written in a conservative form and solved by a finite volume technique to ensure the conservation of the mass of the sediment [*Barbry et al.*, 2000]. The model equations are solved implicitly on the vertical and explicitly on the horizontal direction to avoid a too restrictive limitation on the time step.

[58] The free surface elevation (η) at time t^{n+1} is obtained by solving equation (40). Then the solid volume fraction is computed using the mass conservation equation (5) and the volume conservation (7) gives directly the fluid volume fraction. Depending on the choice of the turbulent model the corresponding equations are solved (see Table 1). Horizontal and vertical momentum equations (6) are computed for the intermediate fluid velocity ($\overrightarrow{u_f^*}$) assuming that the fluid pressure is equal to the fluid pressure at the precedent iteration of the algorithm (p_f^*). The intermediate fluid velocity ($\overrightarrow{u_f^*}$) is then used to solve the Poisson equation for the pressure (37). After that the fluid velocity at time t^{n+1} ($\overrightarrow{u_f^{n+1}}$) is obtained by correcting the intermediate fluid velocity $\overrightarrow{u_f^*}$ with the pressure gradient at time t^{n+1}. Finally, the solid phase velocity at time t^{n+1} ($\overrightarrow{u_s^{n+1}}$) is obtained by solving the momentum equation for the solid phase (6).

$$\Delta\left(\alpha_f^{n+1}p_f^{n+1} - \alpha_f^n p_f^*\right) = -\frac{\rho_f}{\Delta t}\overrightarrow{\nabla}\left(\alpha_f^{n+1}\overrightarrow{u_f^{n+1}} - \alpha_f^n \overrightarrow{u_f^*}\right) \quad (37)$$

[59] The free surface condition is obtained by combining the vertical integrated mass conservation equation for the mixture (38) with the kinematic free surface condition (39).

$$\overrightarrow{\nabla}\cdot\left(\alpha_f\overrightarrow{u_f} + \alpha_s\overrightarrow{u_s}\right) = \overrightarrow{\nabla}\cdot\overrightarrow{u_m} = 0 \quad (38)$$

$\overrightarrow{u_m}$ is the velocity vector of the mixture.

$$\frac{\partial\eta}{\partial t} + u_m|_\eta\frac{\partial\eta}{\partial x} = w_m|_n \quad (39)$$

$u_m|\eta = \alpha_f u_f|_\eta + \alpha_s u_s|_\eta$ and $w_m|_\eta = \alpha_f w_f|_\eta + \alpha_s w_s|_\eta$ represent the horizontal and vertical components of the mixture at the free surface.

$$\frac{\partial\eta}{\partial t} + \frac{\partial Q_m}{\partial x} = 0, \quad (40)$$

where $Q_m = \int_{-h}^{\eta} u_m\, dz$ is the horizontal volume flux of the fluid particle mixture.

4. Physical and Computational Settings

4.1. Experimental Setup

[60] We use the experimental measurements from *Muste et al.* [2005] for comparison with the numerical results. The experiments were conducted using a tilting recirculating flume (L = 6.0 m and B = 0.15 m). The flume's bed was smooth and a flow-conditioning honeycomb was set at the flume's entrance to facilitate quick development of flow turbulence. The flow rate was selected so as to ensure full particle suspension ($U_m \approx 1$ m s^{-1} and $Re \approx 2.10^4$). Channel slope was kept at 0.0113 m/m for all the experiments. Flow depth was small ($H \approx 0.02$ m) so as to have a large channel aspect ratio that prevented the formation of significant secondary flows. All the reported measurements were conducted along the flume centerline, in a test section located 5.3 m downstream the flume's inlet.

[61] Two kinds of sediment particles were used; natural sand (NS) with ρ_s = 2650 kg m^{-3}, and a neutrally buoyant sediment (NBS) consisting of crushed Nylon particles with ρ_s = 1025 ± 5 kg m^{-3}. The NS and NBS particle diameters are 230 ± 20 μm and had practically the same granular shape. Fall velocities are obtained using *Dietrich*'s [1982] formula with d_p = 230 μm and densities of 2650 kg m^{-3} for the NS case and 1025 kg m^{-3} for the NBS case. The physical characteristics of the particles are summarized in Table 2. Three particle concentrations were used in the experiments. In this work we use the measures for the 0.46 10^{-3} volumetric concentration case referred to NS1 and NBS1 hereafter.

[62] The velocity measurements were done by means of particle image velocimetry (PIV) and particle-tracking velocimetry (PTV). Time averages for the various reported quantities were obtained by further taking the mean over all images acquired in a recording series (up to 3500 images).

4.2. Numerical Settings

[63] The simulations are carried out with an 81 × 61 mesh. It is refined vertically near the bottom. The time step is equal to 10^{-3} s for all simulations presented in the following section. The initial condition is set to rest and a first simulation in clear water gives the initial condition for the simulation with sediment.

[64] The boundary conditions are summarized in Table 3. At the inflow boundary (left side), a Neumann condition is imposed for the horizontal velocity of each phase and the free surface elevation is set to zero. At the outflow boundary (right side), a Neumann condition is imposed for the horizontal velocity of each phase and a radiation condition is used for the free surface elevation [*Orlanski*, 1976]. A Neumann condition is imposed for all the other variables, denoted ϕ in Table 3.

[65] At the bottom, a no-slip condition for the fluid phase velocity is imposed ($u_f = 0$) and a slip condition is imposed on the solid phase velocity ($\frac{\partial u_s}{\partial z} = 0$). This condition is justified by the fact that sediment particles are not bounded by viscosity shear as are fluid particles. Therefore, the no-

Table 3. Boundary Conditions

	Inflow	Outflow	Bottom
η	$\eta = 0$	$\frac{\partial \eta}{\partial t} + \sqrt{g \cdot H}\frac{\partial \eta}{\partial n} = 0$	-
u_f	$\frac{\partial u_f}{\partial n} = 0$	$\frac{\partial u_f}{\partial n} = 0$	$u_f = 0$
u_s	$\frac{\partial u_s}{\partial n} = 0$	$\frac{\partial u_s}{\partial n} = 0$	$\frac{\partial u_s}{\partial n} = 0$
w_k	$\frac{\partial w_k}{\partial n} = 0$	$\frac{\partial w_k}{\partial n} = 0$	$w_k = 0$
α_s	$0{,}46\ 10^{-3}$	$\frac{\partial \alpha_s}{\partial n} = 0$	$\frac{\partial \alpha_s}{\partial n} = 0$
ϕ	$\frac{\partial \phi}{\partial n} = 0$	$\frac{\partial \phi}{\partial n} = 0$	-

slip condition at the channel bottom does not apply for the sediment velocity profile.

[66] Boundary conditions for turbulent variables are summarized in (41). The unusual bottom boundary conditions for k_f and ε_f are due to the use of the two-layer model presented above [*Mohammadi and Pironneau*, 1994]

$$\begin{aligned} \textit{Free surface}: &\quad \frac{\partial k_f}{\partial z} = \frac{\partial \varepsilon_f}{\partial z} = \frac{\partial k_s}{\partial z} = \frac{\partial k_{fs}}{\partial z} = 0 \\ \textit{Bottom}: &\quad \frac{\partial k_f}{\partial z} = \frac{\partial \varepsilon_f}{\partial z} = \frac{\partial k_s}{\partial z} = \frac{\partial k_{fs}}{\partial z} = 0 \end{aligned} \tag{41}$$

[67] The shape factor in the c-drag coefficient formulation (12) [*Haider and Levenspiel*, 1989] is equal to 0.6. This value is determined by a comparison with the empirical formulae of *Dietrich* [1982] for the settling of natural particles (see Figure 2).

[68] The restitution coefficient of binary collisions (e) is set to 0.9 for all numerical simulations.

5. Results

[69] In this section, we present the comparison between models results with experimental data of *Muste et al.* [2005] and analytical solutions of *Rouse* [1937] and *Greimann et al.* [1999]. We begin with a clear water simulation to ensure that the hydrodynamic conditions are well simulated by the model. This simulation also gives the initial condition for simulations with particles. Next, we present the model results in terms of the mean velocity, the lag velocity, the volume fraction and the turbulent kinetic energy for the two types of particles (NBS and NS).

5.1. Clear Water Simulation

[70] The steady state results in terms of stream-wise velocity and turbulent correlations for the fluid phase are presented in Figure 3. We point out that at steady state the free surface is parallel to the bottom. We obtain an excellent agreement for the stream-wise velocity Figure 3a. In Figure 3b we compare the turbulent kinetic energy profile obtained by numerical simulation with the measurements. We observe that the numerical profile slightly overestimates the measurements. The numerical prediction for Reynolds stress in Figure 3c shows good agreement with experimental measurements for the diagonal term $\langle u_f' w_f' \rangle_f$. Here again a slight overestimation of the numerical model is observed. A kink is observed on the numerical results. It comes from the transition between the two layers in the turbulence model. A

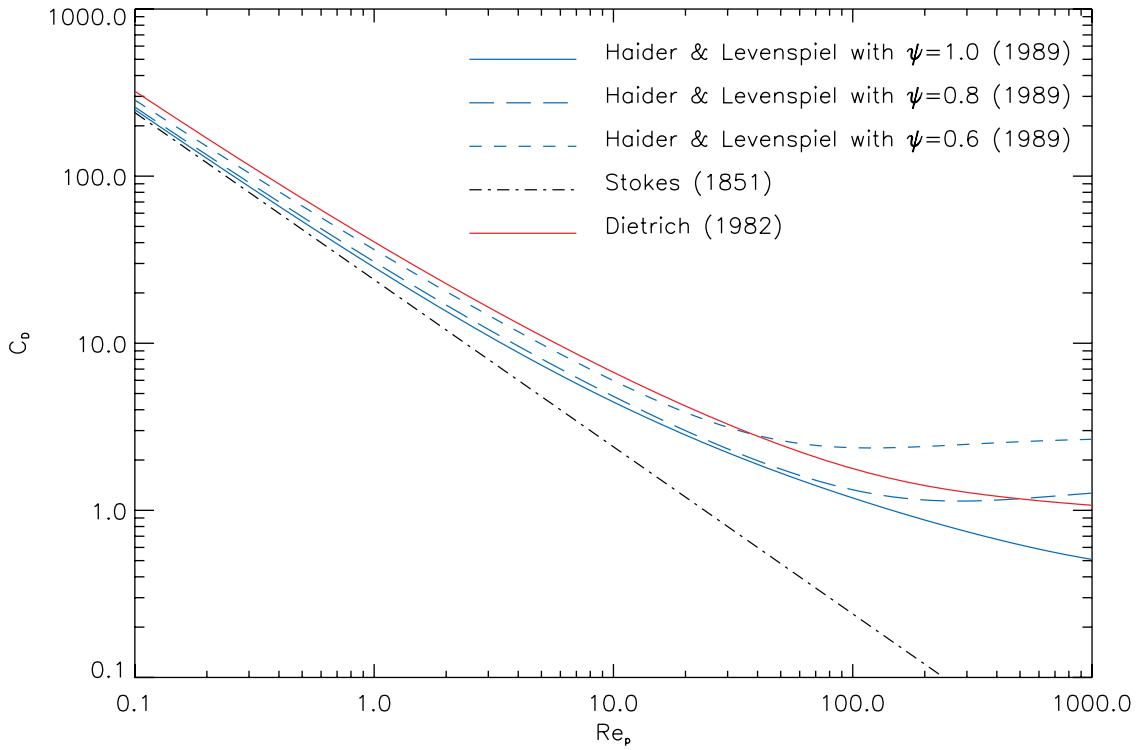

Figure 2. Evolution of the drag coefficient with the particulate Reynolds number. Comparison of the *Haider and Levenspiel* [1989] formula for different values of the shape factor (Ψ = 1, 0.8, and 0.6) with Stokes drag coefficient and the empirical correlation of *Dietrich* [1982].

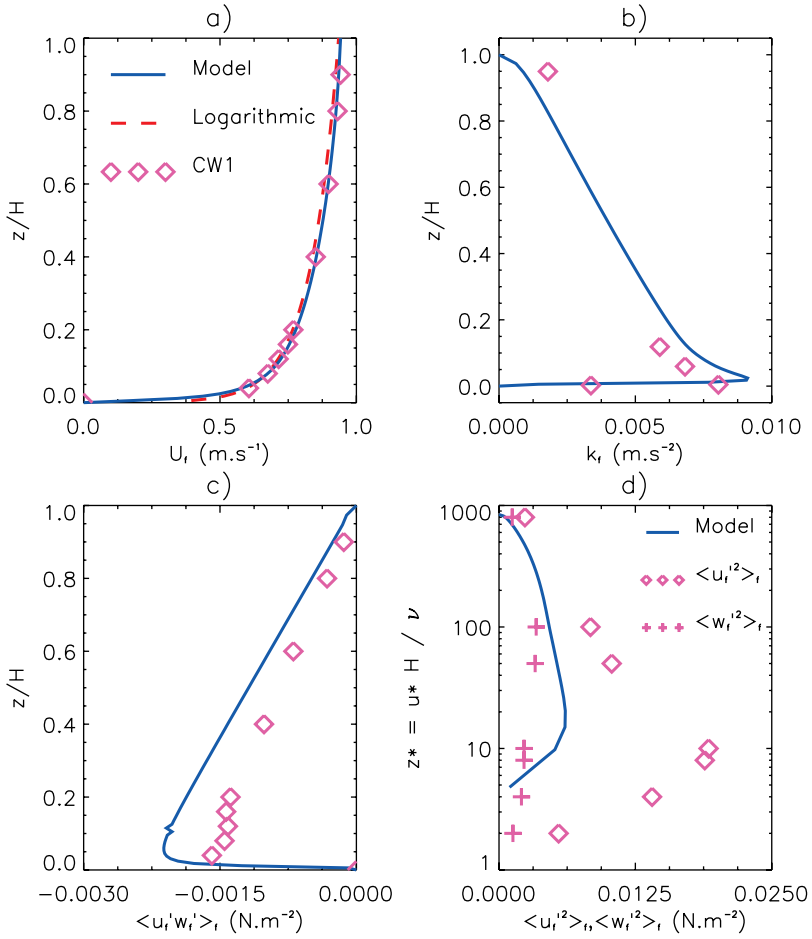

Figure 3. Comparison of numerical results with measurements of *Muste et al.* [2005] in clear water conditions for (a) stream-wise velocity (U_f), (b) Reynolds stress ($\langle u_f' w_f' \rangle_f$), and (c and d) horizontal and vertical turbulent intensities ($\langle u_f'^2 \rangle_f$, $\langle w_f'^2 \rangle_f$).

small variation in the eddy viscosity coupled with a centered derivative for the vertical gradient of horizontal velocity is responsible for the kink. In Figure 3d we obtain an underestimation of the horizontal term $\langle u_f' u_f' \rangle_f$ and an overestimation of the vertical term $\langle w_f' w_f' \rangle_f$ as can be expected with a $k-\varepsilon$ model.

[71] We can estimate the friction velocity (u_*) with the Reynolds stress profile by the same method as the experimental one. This gives the following value $u_* = 0.047$ m s^{-1} which corresponds to a relative error of 12% compared with the measurements. This means that the horizontal pressure gradient is slightly overestimated over the channel in the numerical simulation.

[72] We have performed simulations with particles with the four turbulent models presented in section 2 (see Table 1). We impose a uniform profile for the volume fraction of sediment at the inflow boundary (Table 3) with a mean value of α_s equal to 0.46 10^{-3}, which corresponds to the NBS1 and NS1 cases of *Muste et al.* [2005].

5.2. Mean Horizontal Velocity

[73] Figure 4 shows the mean horizontal velocity profiles obtained with the four turbulence models presented in section 2 compared with the clear water profile. Qualitatively we obtain the same effect of the presence of particles on the mean flow as in the experience [*Muste et al.*, 2005]. We observe an increase of the mean velocity for the NBS particles (Figure 4a) and a decrease of the mean horizontal velocity with the NS particles (Figure 4b).

[74] It should be noted that in Figure 4a the T1 model result differs from the others model results. The drag reduction is observed. In Figure 4b no effect of particles is observed on the mean horizontal velocity profiles with the T3 model.

5.3. Lag Velocity

[75] Figure 5 shows the lag velocity profiles obtained with the four turbulence models presented in section 2 compared with experimental data from [*Muste et al.*, 2005] and analytical solutions of *Greimann et al.* [1999] (see Appendix C) for the NBS1 and NS1 cases. In the NBS1 case (Figure 5a), the velocity lag is negligible far from the bottom and shows negative values in a thin layer near the bottom. *Greimann et al.* [1999] analysis predicts that the lag velocity is of the same order as the fall velocity. In the NBS1 case the particle's inertia is small ($w_{fall} \approx 6.10^{-4}$ m s^{-1}), by consequence the lag velocity is negligible. The negative values near the bottom are due to the difference of

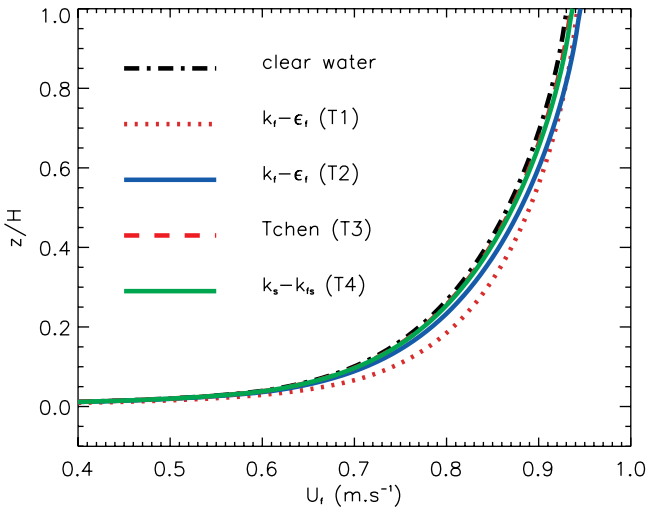

a) NBS1 case.

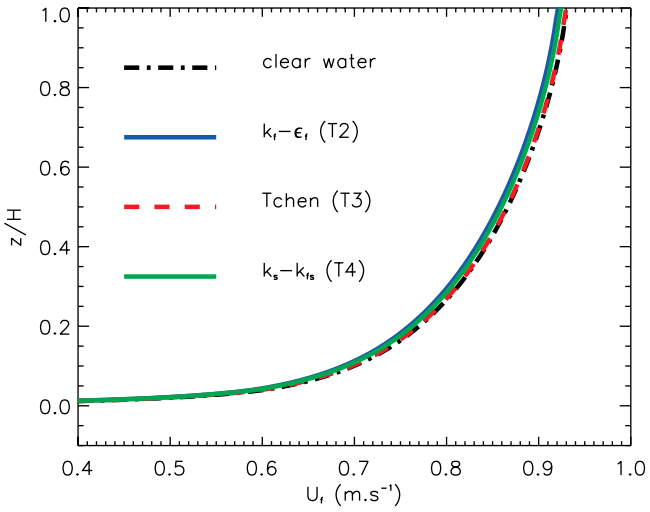

b) NS1 case.

Figure 4. Comparison of the mean horizontal velocity profile for the fluid phase obtained with the four turbulence models (T1, T2, T3, and T4) by numerical simulations with measurements of *Muste et al.* [2005] and analytical solution of *Greimann et al.* [1999] for (a) NBS1 and (b) NS1 cases.

bottom boundary conditions on horizontal velocities of fluid and solid phases. The sediment particles can slip on the wall unlike the fluid. As a result solid particles have a positive velocity in this layer whereas the fluid phase velocity is zero. Consequently the lag velocity ($u_{lag} = u_f - u_s$) is negative.

[76] In the NS1 case (Figure 5b), experimental measurements show negative values for the lag velocity near the bottom with a strong positive vertical gradient. Upward the lag velocity is positive with maximum value of 0.08 m s^{-1} corresponding to approximately 10% of the mean streamwise velocity. The lag velocity decreases toward the free surface where it is negligible. The analytical solution of *Greimann et al.* [1999] predicts the vertical evolution of the lag velocity but the magnitude, in this case, is underestimated by a factor 3. This discrepancy can be explained by the approximation made by *Greimann et al.* [1999] to obtain the analytical solution: inertial effects are neglected. The numerical model qualitatively reproduces the existence of the velocity lag in the NS1 case. But magnitude is greatly underestimated compared with experimental data and analytical solution.

[77] For this last case, the effect of particles on the mean flow can explain the difference between the analytical solution of *Greimann et al.* [1999] and the numerical results. In fact, the *Greimann et al.*'s [1999] analytical solution for the lag velocity is based on the clear water profile unaffected by the presence of particles. Using the same reference for the calculation of the lag velocity (see Figure 6) we obtain a close agreement with the analytical

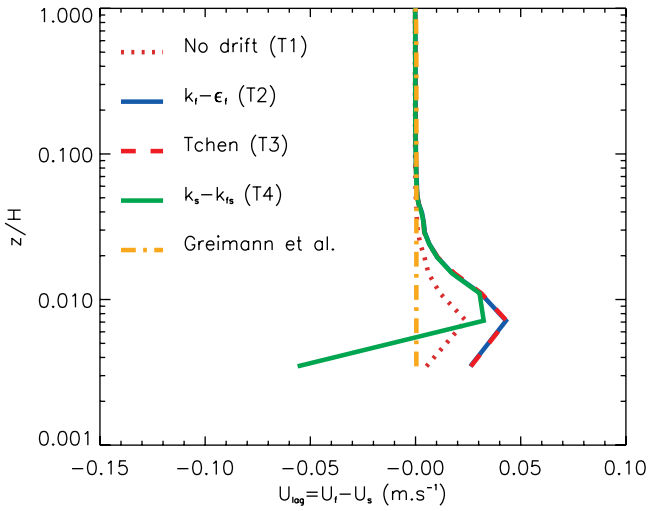

a) NBS1 case.

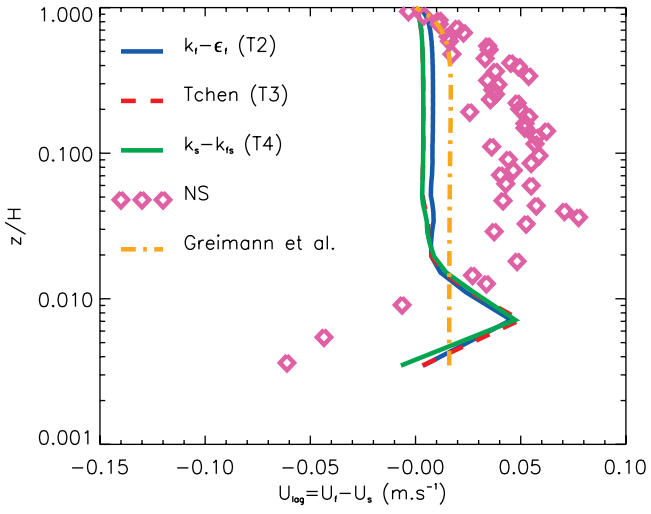

b) NS1 case.

Figure 5. Comparison of the lag velocity profile ($u_{lag} = u_f - u_s$) obtained with the four turbulence models (T1, T2, T3, and T4) by numerical simulations with measurements of *Muste et al.* [2005] and analytical solution of *Greimann et al.* [1999] for (a) NBS1 and (b) NS1 cases.

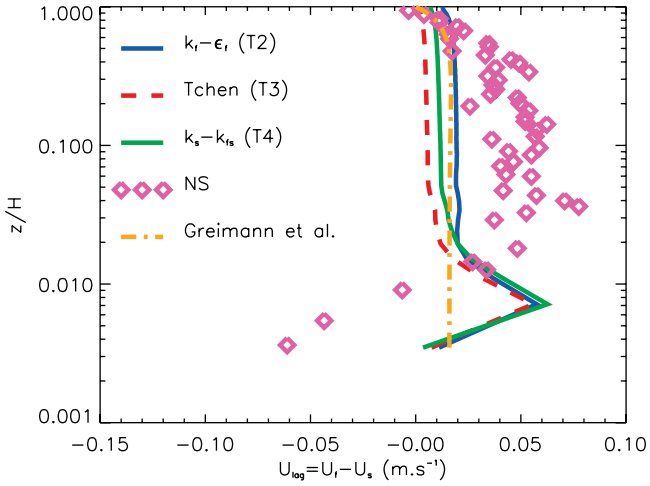

Figure 6. Comparison of the lag velocity profile ($u_{lag} = u_f^{ClearWater} - u_s$) obtained with the three turbulence models (T2, T3, and T4) by numerical simulations with measurements of *Muste et al.* [2005] and analytical solution of *Greimann et al.* [1999] for NS1 case.

solution of *Greimann et al.* [1999] for the T2 model results. The lag velocity obtained with the T4 model is closer to the analytical solution but is always underestimated. Because of the fact that the mean horizontal velocity obtained with the T3 model is quite unaffected by the presence of particles, the lag velocity is unchanged by this mode of calculation.

5.4. Suspended Particle Volume Fraction

[78] In Figure 7, the numerical prediction of the suspended particles volume fraction profiles obtained with the four turbulence models presented in section 2 are compared with experimental data from [*Muste et al.*, 2005] and analytical solutions of *Rouse* [1937] and *Greimann et al.* [1999] (see Appendix C). In the NBS1 case (Figure 7a), sediment particles volume fraction profiles obtained with turbulence models T2, T3 and T4 are close to each other and in good agreement with experimental and analytical profiles. However, when there is no dispersion modeling (model T1) two interfaces appear, one near the bottom between a high concentrated sediment layer and the dilute suspension and the other under the free surface between the dilute suspension and a clear water layer. These characteristics of the sediment particles volume fraction profiles are in disagreement with both experimental and analytical profiles where sediment particles are all maintained in suspension. We point out that the analytical solution of *Greimann et al.* [1999] has not been represented in Figure 7a since it is rigourously identical to the Rouse profile for such low-inertia particles.

[79] In the NS1 case (Figure 7b) the suspended particles volume fraction profile is underestimated with the analytical solution of *Rouse* [1937]. The *Greimann et al.*'s [1999] solution improves upon the *Rouse*'s [1937] formula but fails to represent the suspended particles volume fraction profile. The sediment's volume fraction profile predicted with the model T2 is closer to experimental measurements, especially in the lower part of the channel ($z/H < 0.5$), but also underestimate the suspended particles volume fraction in the upper part of the channel ($z/H > 0.5$). Suspended particles volume fraction profiles obtained numerically with models T3 and T4 are close to each other and are in quite good agreement with the experimental measurements. Results for Model T1 are not presented in Figure 7b because of the unphysical results obtained in the NBS1 case. Moreover we were not able to obtain the convergence for this simulation.

5.5. Fluid Phase Turbulent Kinetic Energy

[80] Figure 8 shows the fluid phase turbulent kinetic energy profiles obtained with the different turbulent models (T1, T2, T3 and T4) compared with the fluid phase turbulent kinetic energy profile obtained in the clear water simulation for the NBS1 and NS1 cases. For the NBS1 case

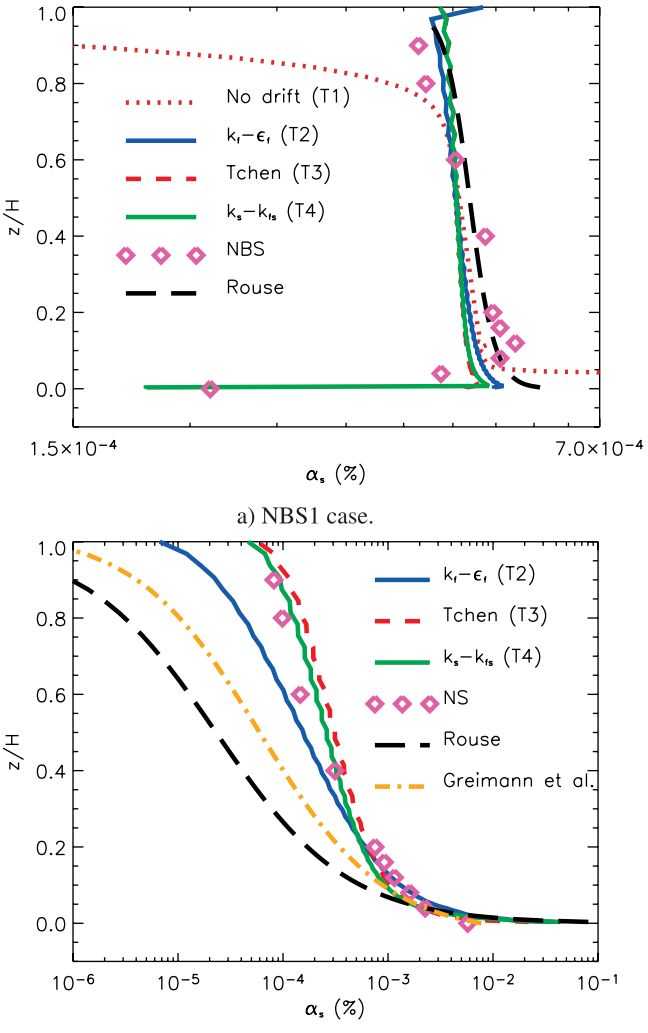

Figure 7. Comparison of the solid volume fraction profile obtained with the four turbulence models (T1, T2, T3, and T4) by numerical simulations with measurements of *Muste et al.* [2005] and analytical profiles of *Greimann et al.* [1999] and *Rouse* [1937] for (a) NBS1 and (b) NS1 case.

(Figure 8a), there is no significant modification of the fluid turbulent kinetic energy profile between the different models (T2, T3 or T4) and the clear water profile. On the other hand for the NS1 case (Figure 8b), we observe some modifications of the fluid phase turbulent kinetic energy profile compared with the clear water profile. In order to quantify these modifications we have calculated the relative variation ($\Delta_r\ k_f$) between the maximum value of the fluid phase turbulent kinetic energy and of the fluid phase turbulent kinetic energy in the clear water case (42) (see Table 4). A slight enhancement of fluid phase turbulent kinetic energy is predicted ($\Delta_r\ k_f < 1\%$) with the three turbulent models T2, T3 and T4 in the NBS1 case. In the NS1 case, the model T2 predicts an increase of fluid phase turbulent kinetic energy, the T3 model shows a very slight decrease of fluid phase turbulent kinetic energy whereas the T4 model predicts a nonnegligible decrease of fluid phase turbulent kinetic energy.

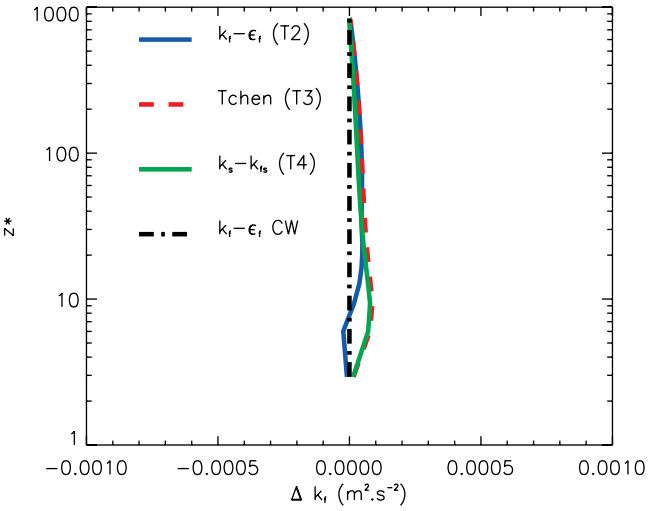

a) NBS1 case.

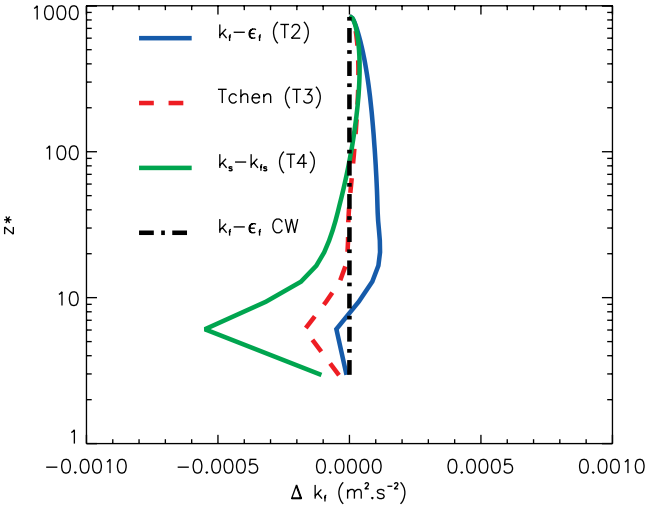

b) NS1 case.

Figure 8. Comparison of the difference of the fluid phase turbulent kinetic energy by reference to the fluid phase turbulent kinetic energy in clear water predicted by simulations with the three turbulence models (T2, T3, and T4) for (a) NBS1 case and (b) NS1 case.

Table 4. Relative Variation of the Fluid Phase Turbulent Kinetic Energy Obtained With Turbulent Models T2, T3, and T4 in the NBS1 and NS1 Cases

	$\Delta_r k_f$ (%)	
	NBS: Crushed Nylon	NS: Natural Sand
Model T2	0.56	+1.35
Model T3	0.90	−0.18
Model T4	0.77	−1.55

$$\Delta_r k_f = \frac{\max\left(k_f\right) - \max\left(k_f^{clear\ water}\right)}{\max\left(k_f^{clear\ water}\right)} \tag{42}$$

6. Discussion

[81] Our results allow us to discuss the improvement of the two-phase flow approach over the classical one. The main difference between these two approaches is the modeling of turbulent motions for both fluid and particles and their cross correlations in the two-phase flow model. The results presented illustrate the importance of these processes in the suspended sediment transport.

6.1. Velocity Profiles

[82] In Figure 4, we have observed a drag reduction on the velocity profile obtained with model T1. This reduction of drag is related to a damping of the fluid turbulence. This can be explained from a simple analysis of the fluid turbulent kinetic energy equation (20). We assume that the flow is steady and one-dimensional, then equation (20) becomes simply:

$$\begin{aligned}
0 &= \frac{\partial}{\partial z}\left(\alpha_f\left(\mu_f + \frac{\mu_f^t}{\sigma_k}\right)\frac{\partial k_f}{\partial z}\right) - \alpha_f\rho_f\epsilon_f + 2\alpha_f\rho_f\nu_f^t\left(\frac{\partial u_f}{\partial z}\right)^2 \\
0 &= \left(\nu_f + \frac{\nu_f^t}{\sigma_k}\right)\frac{\partial k_f}{\partial z}\frac{\partial \alpha_f}{\partial z} + \alpha_f\frac{\partial}{\partial z}\left(\left(\nu_f + \frac{\nu_f^t}{\sigma_k}\right)\frac{\partial k_f}{\partial z}\right) - \alpha_f\epsilon_f \\
&\quad + 2\alpha_f\nu_f^t\left(\frac{\partial u_f}{\partial z}\right)^2 \\
0 &= \frac{1}{\alpha_f}\left(\left(\nu_f + \frac{\nu_f^t}{\sigma_k}\right)\frac{\partial k_f}{\partial z}\right)\frac{\partial \alpha_f}{\partial z} + \frac{\partial}{\partial z}\left(\left(\nu_f + \frac{\nu_f^t}{\sigma_k}\right)\frac{\partial k_f}{\partial z}\right) - \epsilon_f \\
&\quad + 2\nu_f^t\left(\frac{\partial u_f}{\partial z}\right)^2
\end{aligned}$$

[83] The last three terms are classical in single fluid turbulence. They simply express the local equilibrium between production, dissipation and diffusion processes. The first term is originated from the presence of vertical gradient of the fluid volume fraction. This term can be viewed as a Fick-like diffusion process. If we analyze the sign of this term we find that it is negative which means it is a damping term for the fluid turbulent kinetic energy.

$$\begin{cases} \dfrac{1}{\alpha_f}\left(\nu_f + \dfrac{\nu_f^t}{\sigma_k}\right) > 0 \\ \dfrac{\partial k_f}{\partial z} < 0 \\ \dfrac{\partial \alpha_f}{\partial z} = -\dfrac{\partial \alpha_s}{\partial z} > 0 \end{cases} \Rightarrow \frac{1}{\alpha_f}\left(\left(\nu_f + \frac{\nu_f^t}{\sigma_k}\right)\frac{\partial k_f}{\partial z}\right)\frac{\partial \alpha_f}{\partial z} < 0$$

[84] The damping of turbulent kinetic energy is important in the T1 model results for the NBS1 case because of the important vertical gradient of particle concentration as shown in Figure 7a. Since the concentration profile obtained with model T1 is far from the experimental measurements the drag reduction observed on Figure 4 has no physical meaning.

[85] NS1 results confirm that the assumption of horizontal velocity equality between particles and the fluid made in the classical approach is not valid for high-inertia particles. This feature can be represented by a two-phase flow model as described by *Greimann et al.* [1999]. We point out that both the analytical solution [*Greimann et al.*, 1999] and the numerical results underestimate the amplitude of the lag velocity obtained experimentally by *Muste et al.* [2005]. *Greimann et al.*'s [1999] analysis applies to small values of the ratio of the Stokes number over the dimensionless mixing length ($\frac{St_b}{\kappa\sigma} \ll 1$) and neglects inertial effects. Therefore, their analysis cannot represent the lag velocity profile for natural sand particles (NS). In the numerical approach, we have included inertial effects but the lag velocity prediction is not improved. This tends to show that inertial effects are not the processes responsible for the underestimation of the lag velocity. We think that there are two main reasons for the underestimation of the lag velocity. One is the choice of the slip condition for the horizontal velocity of the solid phase. This condition implies that collisional and frictional effects at the wall are neglected. The mean horizontal velocity of the solid phase should be slower and the lag velocity would be greater. The second reason is the isotropic assumption induced by the use of a k-ε type turbulence model. As illustrated by Figure 3, the normal Reynolds stresses are not isotropic. Moreover, the dispersion tensor in the drift velocity definition is also anisotropic, the crossing-trajectories effects vary with the orientation of the relative motion of particles with the mean flow direction. To take into account the anistropy of turbulence, we shall use a second-order turbulence model that is beyond the scope of this paper.

[86] The two-phase models results underestimate the amplitude of the lag velocity predicted by the analytical solution of *Greimann et al.* [1999]. But we have shown that the choice of the reference for the mean horizontal velocity of the fluid phase affect the lag velocity profile. When taking the clear water profile as reference, the lag velocity obtained with the T2 model is in close agreement with the analytical solution of *Greimann et al.*'s [1999]. This allows us to validate the proposed numerical approach for the lag velocity simulation.

[87] An important point to discuss is the modeling of the dispersion tensor in the expression of the drift velocity (14). We demonstrate, on the basis of physical considerations, that the modeling of the dispersion in tensor formulation is essential for representation of the lag velocity. *Muste et al.* [2005], *Sumer and Deigaard* [1981] and *Rashidi et al.* [1990], amongst others, have shown experimentally that the lag velocity is positive when sufficiently far from the bed. *Greimann et al.*'s [1999] have shown, theoretically, that the lag velocity equals the opposite of the horizontal drift velocity: $U_{lag} = -u_d + o(\tau_{fs})$. Therefore, the horizontal drift velocity value must be negative to be consistent with the experimental evidence: $u_d < 0$. The horizontal drift velocity is assumed to be as described by *Simonin* [1991]: $u_d = -D^t_{fs,xz}\frac{\partial \alpha_s}{\partial z}$ (14). The vertical gradient of the sediment's particle volume fraction is negative $\frac{\partial \alpha_s}{\partial z} < 0$ meaning that the sediment's particle volume fraction is increasing toward the bed. So the dispersion coefficient $D^t_{fs,xz}$ must be negative to satisfy the sign of the lag velocity observed experimentally. If we make the isotropic assumption to obtain the dispersion coefficient, that is $\overline{\overline{D^t_{fs}}} = \nu^t_{fs}\tau^t_{fs}\overline{\overline{I}}$, then the sign condition for $D^t_{fs,xz}$ is not fulfilled and the lag velocity would be negative. However, if we use a tensor formulation to express the cross-correlation tensor (Boussinesq model) in the dispersion coefficient expression $\overline{\overline{D^t_{fs}}}\left\langle \overrightarrow{u'_f} \otimes \overrightarrow{u'_s} \right\rangle_s \tau^t_{fs}$ (31), the term $\langle u'_f w'_s \rangle_s$ is negative and the horizontal drift velocity satisfies the sign condition. This analysis shows that one must use the tensor formulation to calculate the dispersion coefficient in the drift velocity formulation (14), otherwise the lag velocity between fluid and particles will not be consistent with experimental and theoretical results.

6.2. Sediment Volume Fraction Profile and Turbulence Analysis

[88] In model T1, there is no other suspension mechanism than the non-Newtoninan stress. This term is responsible for the presence of particles in suspension. The fact that the sediment volume fraction profile obtained with model T1 is far from the experiments shows that the modeling of the dispersion of particles by the fluid turbulent motion is of primary importance. We show that the introduction of a drift velocity in the momentum transfer term in equation (6) permits the description of the physical processes of dispersion of particles by the fluid turbulent motion. The utility of this approach is confirmed by the results obtained with models T2, T3 and T4. When the inertia of the particles is small (NBS1 case) we obtain results similar to the classical approach [*Rouse*, 1937] and to the analytical solution of *Greimann et al.* [1999] with these three turbulent models. When inertia of the particles is larger, as in the NS1 case, the single phase flow model fails to reproduce the sediment volume fraction profile [*Rouse*, 1937] whereas the two-phase flow analytical solution [*Greimann et al.*, 1999] gives a more accurate description. Results obtained with the model T2 give a more accurate prediction of the sediment volume fraction profile but show some discrepancies with the experimental measurements for $z/H > 0.5$. However when turbulent models for solid phase and fluid particle turbulent interactions are considered (model T3 and T4) the sediment volume fraction profile predicted by the numerical simulation is close to the one obtained with experimental measurements.

6.3. Governing Equations and Turbulence Modeling

[89] We discuss the difference between the analytical solution of *Greimann et al.* [1999] and the present model. The main difference between the governing equations of these two approaches concerns the modeling of the turbulent stress terms, *Greimann et al.* [1999] assume that solid phase turbulent intensities are constant and equal to the near-bottom value of the fluid phase turbulent intensities predicted by the theoretical profile of *Nezu and Rodi* [1986]. They neglect the effect of the particles on the fluid turbulence. The other assumptions used by *Greimann et al.*'s [1999] to derive their model are equivalent to the model T2.

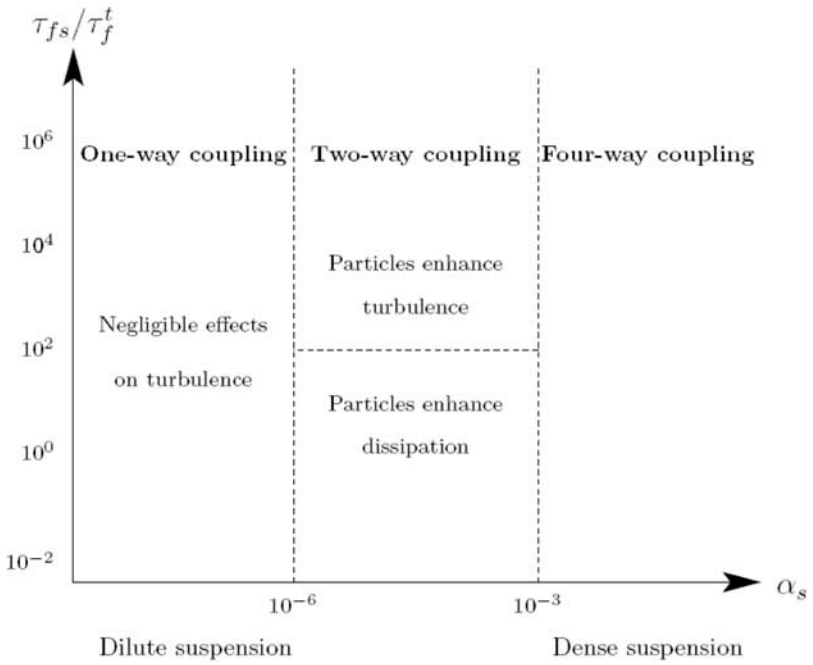

Figure 9. Classification of flow regimes for gas-solid flows according to *Elghobashi* [1991].

The improvement of the sediment volume fraction profile obtained with the model T2 is mainly attributed to this difference in the modeling of the turbulent stress terms. Another difference concerns the numerical resolution of the governing equations in model T2. Concerning the governing equations for model T2 and models T3 and T4, we can identify three fundamental differences. The first one is the modeling of the turbulent stress tensor for the solid phase: $\overline{\overline{T_s^{Re}}}$; in model T2 we assume that $\overline{\overline{T_s^{Re}}} = \overline{\overline{T_f^{Re}}}$. The second one is the modeling of the dispersion coefficient in the drift velocity expression: $\overline{\overline{D_{fs}^t}}$. The third one is the modeling of the fluid turbulent kinetic energy transfer term in the $k_f - \varepsilon_f$ model: Π_{kf}. To further discuss the difference between model T2 and models T3 and T4 prediction for the sediment volume fraction profile we analyze the results from the models in terms of the fluid phase turbulent kinetic energy profile.

[90] *Elghobashi* [1991] proposed a classification for gas-solid suspensions based on some characteristic time scales (Figure 9). Figure 10 shows the ratio of the relaxation time scale τ_{fs} on the fluid turbulent time scale seen by the particles τ_{fs}^t and the ratio of the relaxation time scale τ_{fs} on the particle-particle collision time scale τ_s^c for the NBS1 and the NS1 cases. The ratio of the relaxation time scale τ_{fs} on the fluid turbulent time scale seen by the particles τ_{fs}^t is always lower than 10^2. According to *Elghobashi*'s [1991] classification the effects of particles on the turbulent motion of the fluid phase can be observed. Here we observe a damping of fluid turbulent kinetic energy NS1 in the cases.

[91] As seen in Figure 8 the fluid turbulent kinetic energy is slightly enhanced far from the bed ($z^* > 10$-100 for NS1) for the NS1 case and at all depths for the NBS1 case. Figure 8b also shows that damping of fluid turbulent kinetic energy occurs near the bed ($z^* > 10$-100) in the NS1 case.

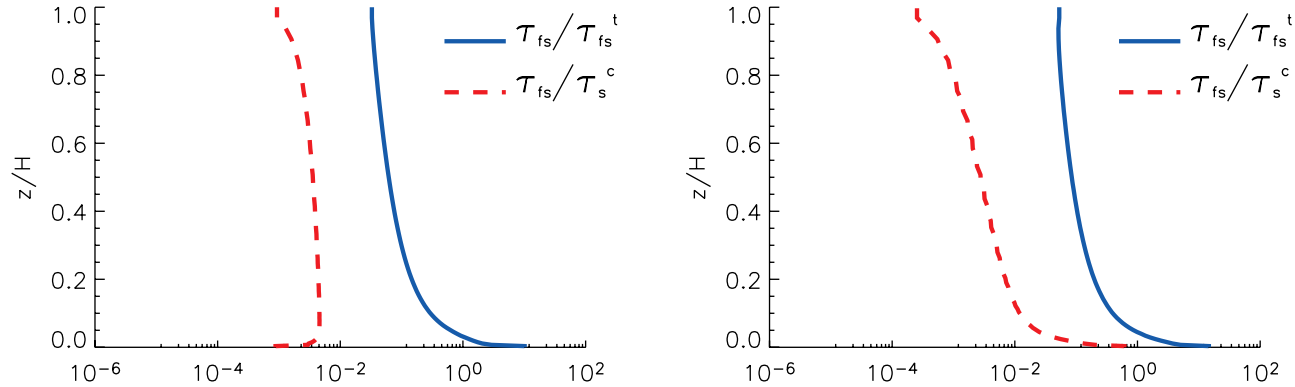

Figure 10. Ratio of different characteristic time scales predicted by the $k_s - k_{fs}$ model (T4) for (a) the NBS1 case and (b) the NS1 case.

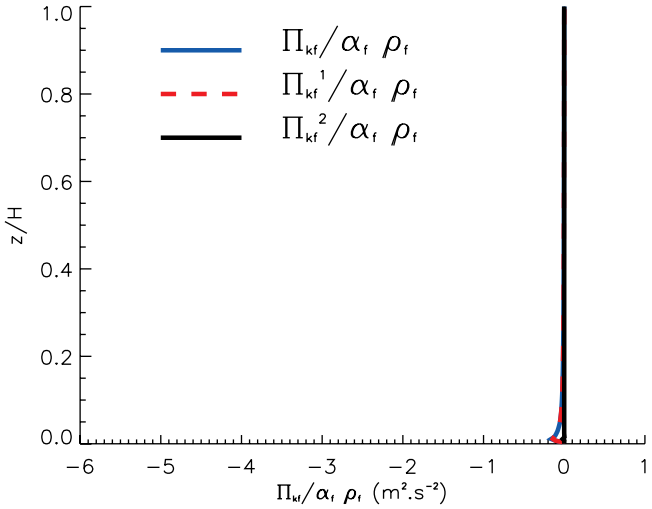

a) T3 model.

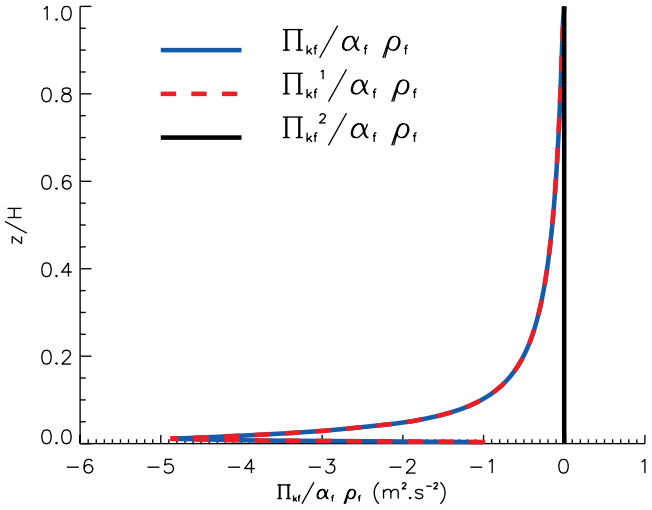

b) T4 model.

Figure 11. Profile of the interaction term for the fluid turbulent kinetic energy ($\Pi_{k_f \text{ with } \Pi k_f}{}^1 = \frac{\alpha_f \rho_f}{\tau_{fs}}(-2\ k_f + k_{fs})$ and $\Pi_{k_f}{}^2 = \frac{\alpha_f \rho_f}{\tau_{fs}} \overrightarrow{u_d}.\overrightarrow{u_r}$) obtained with turbulence models (a) T3 and (b) T4 for NBS1 case.

For this case, models T3 and T4 predict a significant damping of the fluid turbulent kinetic energy whereas the T2 model predicts a relatively small damping of fluid turbulent kinetic energy for in a very small region near the bottom ($z^* > 10$). In order to see whether the transfer term of fluid turbulent kinetic energy (23) is a damping or a production term of turbulence, we have plotted in Figures 11 and 12 the vertical profiles of the two contributions of the interphase transfer term (23) for model T3 and T4 in both NBS1 and NS1 cases. It appears that both contributions induce a damping of fluid turbulent kinetic energy. The Work done by the drag force associated with the fluid turbulent motion ($\Pi_{k_f}{}^2 = \frac{\alpha_f \rho_f}{\tau_{fs}} \overrightarrow{u_d} \cdot \overrightarrow{u_r}$) is a damping term for the NS1 case (see Figure 12). Whereas in the NBS1 case this contribution is negligible because of the very small relative velocity. The other contribution appearing in equation (23) ($\Pi_{k_f}{}^1 = \frac{\alpha_f \rho_f}{\tau_{fs}}(-2\ k_f + k_{fs})$) also leads to a damping of fluid turbulent kinetic energy for both NBS1 and NS1 cases. This means that the transfer of fluctuating energy is done from the fluid to the particles: particles are shaken by the fluid turbulent motion. These results show that the damping of fluid turbulence arises mainly from a kinetic transfer between fluid and particles and not from the drag at the scale of the particles. The other interesting point is that the enhancement of fluid turbulent kinetic energy is not due to this transfer of turbulent kinetic energy. In fact, it can be due to an increase of the turbulent kinetic energy production induced by an increase of the vertical gradient of the fluid velocity or it can be due to a decrease of dissipation of fluid turbulent kinetic energy (ε_f) due to the presence of the transfer term in equation (21).

7. Conclusion

[92] In this paper a study of the turbulent effect on sediment transport in an open channel flow has been done

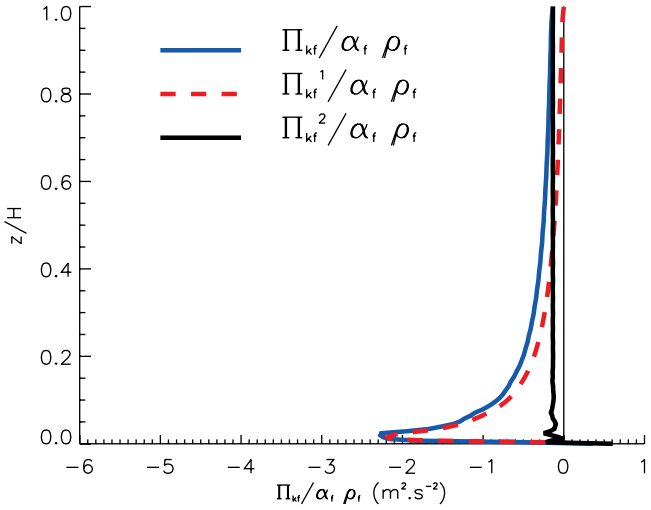

a) T3 model.

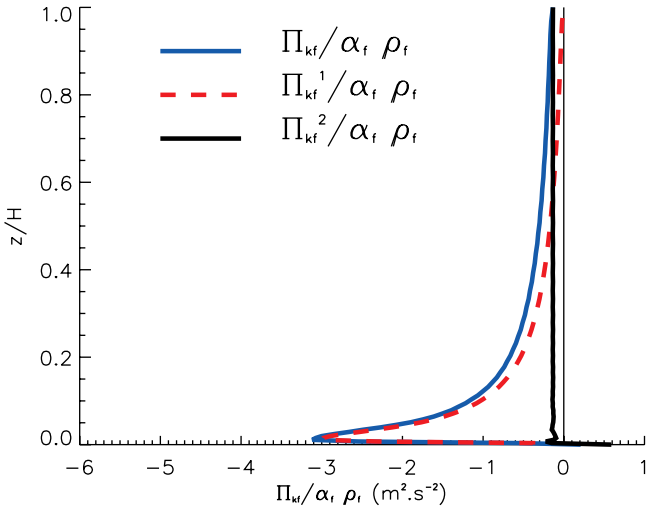

b) T4 model.

Figure 12. Profile of the interaction term for the fluid turbulent kinetic energy ($\Pi_{k_f \text{ with } \Pi k_f}{}^1 = \frac{\alpha_f \rho_f}{\tau_{fs}}(-2\ k_f + k_{fs})$ and $\Pi_{k_f}{}^2 = \frac{\alpha_f \rho_f}{\tau_{fs}} \overrightarrow{u_d}.\overrightarrow{u_r}$) obtained with turbulence models (a) T3 and (b) T4 for NS1 case.

with a 2-D XZ two-phase flow model. We have focused our attention on turbulent closures. Simulations of dilute sediment laden flows have been performed and compared with experimental data with two types of particles with different inertia [*Muste et al.*, 2005]. Different turbulent closures have been tested (models T1, T2, T3 and T4) and their relevance in terms of physical processes modeling have been discussed.

[93] The principal conclusions are as follows:

[94] 1. Modeling dispersion of particles by the fluid turbulent motion in the momentum equations by a drift velocity model [*Simonin*, 1991] allows representation of the physical processes of dispersion of particles by the fluid turbulent motion in both the vertical direction (suspension mechanism) and in the horizontal direction (velocity lag).

[95] 2. A two-phase flow model including turbulent closures for solid phase turbulence (model T3 and T4) is appropriate for representing the main features of the sediment laden flow: the existence of a horizontal velocity lag between the particles and the fluid; the increase of the dispersion effects of particles with their inertia, and the damping of fluid turbulent kinetic energy. We have shown that the damping of fluid turbulent kinetic energy is represented in the model as a transfer of fluctuating kinetic energy from the fluid to the particles.

[96] 3. An algebraic closure for solid phase turbulence and fluid particle turbulent interactions (model T3) is a good compromise between representing the physical processes and complexity.

[97] In this approach no empirical parameter was adjusted to obtain a satisfactory concentration profile. This constitutes a real improvement upon the classical sediment transport modeling approach (passive scalar hypothesis). Nevertheless, our approach is time consuming and cannot be applied on a large scale. This is a first step in the development of a turbulent two-phase flow model for sediment transport. Future work will be concerned with the analysis of these results in terms of the solid phase momentum and fluid phase turbulent kinetic energy balance to provide guidelines for the development of parameterizations for classical suspended sediment transport modeling.

[98] Finally, for actual use, an algebraic closure for the solid phase fluctuating motion and fluid particle turbulent interactions (model T3) is a good compromise between representation of the physical processes and complexity of implementation. This simple model gives quite similar results to the first-order model (model T4) where two additional transport equations have to be solved. This approach could be used to test closures for two-phase semianalytical solutions and for full numerical solution for sediment transport in a simple and effective way for steady state regime.

Appendix A: Two-Layer $k - \varepsilon$ Model

[99] In the two-layer $k - \varepsilon$ model the computational domain is split in two layers, the high Reynolds number area and the low Reynolds number area. In the first layer, the standard $k - \varepsilon$ model is applied. In the near wall region, the low Reynolds number layer, the dissipation of fluid phase turbulent kinetic energy ε_f and the eddy viscosity ν_f^t are imposed by algebraic relationships as follows:

$$\varepsilon_f = \frac{k_f^{3/2}}{l_\varepsilon} \tag{A1}$$

and

$$\nu_f^t = c_\mu \sqrt{k_f} l_\mu, \tag{A2}$$

where l_μ and l_ε represent two length scales that account for the damping of turbulence in the near-wall region.

$$l_\mu = \kappa c_\mu^{-3/4} z \left(1 - e^{-\frac{z^+}{z_0}}\right) \tag{A3}$$

$$l_\varepsilon = \kappa c_\mu^{-3/4} z \left(1 - e^{-\frac{z^+}{2\kappa c_\mu^{-3/4}}}\right) \tag{A4}$$

[100] The local Reynolds number $z^+$is defined by: $z^+ = \frac{\sqrt{k_f} z}{\nu_f}$. It is based on k_f rather than u^*. The separation between the two layers is fixed at $z^+ = 70$.

Appendix B: Closures for the $k_s - k_{fs}$ Model

[101] In this appendix we present the detailed expressions for the kinetic and collisional diffusivity K_s^t (B1) and K_s^c (B4) obtained in the frame of the kinetic theory for granular flow [*Balzer et al.*, 1995; *Jenkins and Richman*, 1985].

$$K_s^t = \frac{\frac{1}{3}\tau_{fs}^t k_{fs} + \frac{5}{9}\tau_{fs}\frac{2}{3}k_s(1+\alpha_s g_0 \phi_c)}{1 + \frac{5}{9}\tau_{fs}\frac{\zeta_c}{\tau_s^c}} \tag{B1}$$

where the constants ϕ_c and ζ_c are given by: $\phi_c = 3(1+e)^2(2e-1)/5$ and $\zeta_c = (1+e)(49-33e)/100$. g_0 is the radial distribution function which accounts for the increase in the probability of collisions when the gas becomes denser. In a very diffuse gas, g_0 equals one, whereas g_0 tends to infinity when the particles are closely packed. The formulation proposed by *Ma and Ahmadi* [1986] is valid in dense cases and has been used in this model (B2).

$$g_0 = \frac{1 + 2.5\alpha_s + 4.5904\alpha_s^2 + 4.515439\alpha_s^3}{\left(1 - \left(\alpha_s/\alpha_s^{\max}\right)\right)^{0.678021}} \tag{B2}$$

τ_s^c is the interparticle collision time scale and is given by (B3) in the framework of the kinetic theory of granular flow.

$$\tau_s^c = \frac{d}{24 g_0 \alpha_s}\sqrt{(3\pi)/(2k_s)} \tag{B3}$$

$$K_s^c = \alpha_s g_0 (1+e)\left(\frac{6}{5}K_s^t + \frac{4}{3}d\sqrt{\frac{2k_s}{3\pi}}\right) \tag{B4}$$

Appendix C: Analytical Solutions of *Greimann et al.* [1999]

[102] In this appendix we briefly present analytical solutions of *Greimann et al.* [1999] for the concentration

profile (C2) and the lag velocity (C4). The authors assumed that the concentration of particles is sufficiently small so the vertical turbulent intensities can be specified according to the experimental work of *Nezu and Rodi* [1986] for clear water conditions:

$$\overline{w_f'^2} = u_*^2 C_\nu e^{-1.34\sigma}, \tag{C1}$$

where $C_\nu = 1.51$ is a constant.

[103] The analytical model for the volume fraction profile is obtained by assuming that turbulence intensities are constant with depth through the flow and are equal to their value in the near wall region: $\overline{w_f'^2} = \overline{w_s'^2} = u_*^2 C_\nu$. The volume fraction profile is given by the following equation:

$$\frac{\alpha_s}{\alpha_s^a} = \left[\frac{\sigma - \frac{1}{2}(1+S')}{\sigma - \frac{1}{2}(1-S')}\,\frac{\sigma^a - \frac{1}{2}(1+S')}{\sigma^a - \frac{1}{2}(1-S')}\right]^{r_e/S'}, \tag{C2}$$

with

$$S' = \sqrt{1 + \frac{4C_\nu St_b}{\gamma_s \kappa}} \quad ; \quad r_e = \frac{w_s}{\gamma_s \kappa u_*} \tag{C3}$$

[104] α_s^a is the reference volume fraction at the adimensionalized height σ_a above the bed. $\gamma_s = [1 + C_\beta \cdot (3\,\|\overrightarrow{u_r}\|^2)/(2kf)]^{-1/2}$ accounts for the loss of correlation between the turbulent motions of fluid and particles due to the relative motion of solid particles, this processes has been described by *Csanady* [1963] as the crossing-trajectory effect. $\overrightarrow{u_r} = \overrightarrow{u_s} - \overrightarrow{u_f}$ is the mean relative velocity between phases, k_f is the fluid turbulent kinetic energy and C_β is a constant. $St = \frac{\tau_{fs}}{\tau_{fb}}$ represent the Stokes number with $\tau_{fs} = \frac{w_s \rho_s}{g(\rho_s - \rho_f)}$ the particle relaxation time scale and $\tau_{fb} = \frac{u_*}{H}$ a characteristic time scale of the fluid flow based on the bottom shear velocity. When $St = 0$ and $\gamma_s = 1$ the solution of *Greimann et al.* [1999] is equivalent to the *Rouse* [1937] profile (4).

[105] Assuming that $\frac{St_b}{\kappa\sigma} \ll 1$ *Greimann et al.* [1999] derived the following analytical solution for the lag velocity:

$$U_{lag} = U_f - U_s = \frac{2}{3} w_s (1-\sigma) e^{1.34\sigma}. \tag{C4}$$

[106] This model predicts that for relatively small particles away from the bed, U_{lag} is of the order of the settling velocity and decreases to zero at the free surface. This is in agreement with experimental data from *Muste and Patel* [1997] and *Kaftori et al.* [1996].

Notation

Roman notation

A_p Surface area of the real particle, m^2.
A_s Surface area of the equivalent spherical particle, m^2.
C_D Drag coefficient, Ø.
C_β Empirical constant for crossing trajectory effect, Ø.
c Mass concentration of sediment particles, kg m^{-3}.
d_{ip} Interparticular distance, m.
d_p Particle's diameter, m.
$\overline{\overline{D}}_k$ Mean strain rate tensor of phase k, s^{-1}.
$\overline{\overline{D}}_{fs}^t$ Dispersion tensor for the drift velocity, m^2 s^{-1}.
e Restitution coefficient of binary collisions, Ø.
$\overrightarrow{g}$ Gravitational acceleration, m s^{-2}
g_0 Radial distribution function, Ø.
H Water depth, m.
$\overline{\overline{I}}$ Unit tensor, Ø.
k_f Fluid phase turbulent kinetic energy, m^2 s^{-2}.
k_s Solid phase turbulent kinetic energy, m^2 s^{-2}.
k_{fs} Fluid particle velocity covariance, m^2 s^{-2}.
l_ε Length scale for the fluid turbulent kinetic energy dissipation in the near wall region (2 layer model), m.
l_μ Length scale for the fluid eddy viscosity in the near wall region (2 layer model), m
$\overrightarrow{M_k}$ Interfacial momentum transfer term, kg m^{-2} s^{-2}.
$\overrightarrow{M_k'}$ Force exerted by the other phase on phase k (drag, virtual mass, lift,...), kg m^{-2} s^{-2}.
$\overrightarrow{n}$ Normal unit vector, Ø.
p_k Pressure in phase k, Pa.
p_{ki} Interfacial pressure for phase k, Pa.
p_s^{eff} Effective pressure for solid phase, Pa.
p_k^t Turbulent pressure for phase k, Pa.
Re Reynolds number, Ø.
Re_p Mean particle Reynolds number, Ø.
S' Exponent correction in the analytical solution for the particle volume fraction profile of *Greimann et al.* [1999]
St Stokes number, Ø.
t Time, s.
$\overline{\overline{T}}_k$ Strain tensor of phase k, N m^{-2}.
$\overline{\overline{T}}_k^{Re}$ Turbulent strain tensor of phase k, N m^{-2}.
$\langle\overrightarrow{u_k}\rangle_k$, $\langle u_{k,i}\rangle_k$ Mean velocity vector, ith component of the velocity vector of phase k, m s^{-1}.
$\overrightarrow{u_k'}$, $u_{k,i}'$ Fluctuating velocity vector, ith component of the fluctuating velocity vector of phase k, m s^{-1}.
$\overrightarrow{u_r}$, $u_{r,i}$ Relative velocity vector, ith component of the relative velocity vector between phases, m s^{-1}.
$\overrightarrow{u_d}$, $u_{d,i}$ Drift velocity vector, ith component of the drift velocity vector, m s^{-1}.
U_{lag} Lag velocity, m s^{-1}.
u_* Bottom shear velocity, m s^{-1}.
w_s Sediment's particle velocity, m s^{-1}
$\overrightarrow{x}$, x_i Position vector, ith component of the position vector, m.

Greek notation

α_k Volume fraction of phase k, Ø.
$\alpha_s^{\max}$ Maximum volume fraction of solid phase, Ø.
α_s^0 Reference volume fraction of solid phase, Ø.
β Amplification factor for the viscosity, Ø.

ε_k Turbulent kinetic energy dissipation of phase k, $m^2\ s^{-3}$.
ε_{fs} Fluid particle covariance dissipation, $m^2\ s^{-3}$
ζ_s Bulk viscosity, $m^2\ s^{-1}$.
η Free surface elevation, m.
κ Von Karman constant, Ø.
ν_k Kinematic viscosity of phase k, $m^2\ s^{-3}$.
ν_k^t Eddy viscosity of phase k, $m^2\ s^{-3}$.
ν_{fs}^t Fluid particle covariance eddy viscosity, $m^2\ s^{-3}$.
ν_s^c Collisional viscosity of solid phase, $m^2\ s^{-3}$.
ξ Ratio of the fluid turbulence time scale seen by the particles over the particle relaxation time, Ø.
ρ_k Solid phase density, $kg\ m^{-3}$.
σ Adimensionalized depth, Ø.
σ_0 Reference adimensionalized depth for analytical profiles [*Rouse*, 1937; *Greimann et al.*, 1999], Ø.
$\overline{\overline{\tau}}_k$ Deviatoric component of the stress tensor of phase k, $N\ m^{-2}$.
$\overline{\overline{\tau}}_{ki}$ Deviatoric component of the interfacial stress tensor of phase k, $N\ m^{-2}$.
τ_{fs} Particle relaxation time, s.
τ_f^t Fluid turbulence time scale, s.
τ_{fs}^t Fluid turbulence time scale seen by the particles, s.
τ_s^c Binary collisions time scale, s
τ_{fb} Bulk integral fluid time scale, s.
Ψ Shape factor, Ø.

[107] **Acknowledgments.** The authors acknowledge the CETMEF (Centre d'Etude Technique Maritime et Fluvial/French center for marine and fluvial technical studies, contract 05-510006-000-228-6034) and the European Commission (FLOCODS Project, FP5-contract ICA4-CT2001-10035) for the financial support of the thesis of J. Chauchat. Computational tasks for this study required the resources of the CRIHAN (Centre de Ressources Informatique de Haute Normandie/Normandy computer resources center). The first author would like to thank J.-C. Brun-Cottan for the fruitful discussion on sediment transport processes during his Ph.D.

References

Amoudry, L., T.-J. Hsu, and P. L.-F. Liu (2005), Schmidt number and near-bed boundary condition effects on a two-phase dilute sediment transport model, *J. Geophys. Res.*, *110*, C09003, doi:10.1029/2004JC002798.

Balzer, G., A. Boëlle, and O. Simonin (1995), Eulerian gas-solid flow modelling of dense fluidized bed, in *Fluidization VIII: Proceedings of the Eighth Engineering Foundation Conference on Fluidization, May 14–19, 1995, Tours, France*, pp. 1125–1134, Eng. Found., New York.

Barbry, N. (2000), Modélisation du transport sédimentaire en milieux estuariens selon une approche diphasique (fluide-particule), Ph.D. thesis, Univ. de Caen, Caen, France.

Barbry, N., S. Guillou, and K. D. Nguyen (2000), Une approche diphasique pour le calcul du transport sédimentaire en milieux estuariens, *C.R. Acad. Sci. Ser. IIb Mec. Phys. Astron.*, *328*, 793–799.

Boëlle, A., G. Balzer, and O. Simonin (1994), Application d'une modélisation à deux fluides à la prédiction des lits fluidisés denses, *He-44/94/017a*, Lab. Natl. d'Hydraul., Chatou, France.

Chapman, S., and T. G. Cowling (1970), *The Mathematical Theory of Non-uniform Gases*, Cambridge Univ. Press, Cambridge, U.K.

Chauchat, J. (2007), Contribution à la modélisation diphasique du transport sédimentaire en milieux ctiers et estuariens, Ph.D. thesis, Univ. de Caen, Caen, France.

Chorin, A. J. (1968), Numerical simulation of Navier-Stokes equations, *Math. Comput.*, *22*, 745–762.

Coleman, N. L. (1970), Flume studies of the sediment transfer coefficient, *Water Resour. Res.*, *6*, 801–809.

Csanady, G. (1963), Turbulent diffusion of heavy particles in the atmosphere, *J. Atmos. Sci.*, *20*, 201–208.

Deutsch, E., and O. Simonin (1991), Large eddy simulation applied to the motion of particles in stationary homogeneous fluid turbulence, *Turbulence Modification in Multiphase Flows*, *FED Ser.*, vol. 110, pp. 35–42, Am. Soc. Mech. Eng., New York.

Dietrich, W. E. (1982), Settling velocity of natural particles, *Water Resour. Res.*, *18*, 1615–1626.

Drew, D. A. (1976), Production and dissipation of energy in the turbulent flow of a particule-fluid mixture, with some results on drag reduction, *J. Appl. Mech.*, *43*, 543–547.

Drew, D. A. (1983), Mathematical modelling of two-phase flow, *J. Appl. Mech.*, *15*, 261–291.

Drew, D. A. (2001), A turbulent dispersion model for particles or bubbles, *J. Eng. Math.*, *41*, 259–274.

Drew, D. A., and R. T. Lahey (1993), Analytical modelling of multiphase-flow, in *Particulate Two-Phase Flows*, chap. 16, pp. 509–566, Butterworth-Heinemann, Boston, Mass.

Duy, N. T., and T. Shibayama (1997), A convection-diffusion model for suspended sediment in the surf zone, *J. Geophys. Res.*, *102*, 23,169–23,186.

Einstein, A. (1906), Eine neue bestimmung der molekuldimensionen, *Ann. Phys.*, *19*, 289–306.

Elghobashi, S. (1991), Particle-laden turbulent flows: Direct simulation and closure models, *Appl. Sci. Res.*, *48*, 301–314.

Elghobashi, S., and T. Abou-Arab (1983), A two-equation turbulence model for two-phase flows, *Phys. Fluids*, *26*, 931–938.

Enwald, H., E. Peirano, and A.-E. Almstedt (1996), Eulerian two-phase flow theory applied to fluidization, *Int. J. Multiphase Flow*, *22*, 21–66.

Favre, A. (1965), Equations des gaz turbulents compressibles, *J. Mec.*, *4*, 361–390.

Frankel, N. A., and A. Acrivos (1967), On the viscosity of a concentrated suspension of solid spheres, *Chem. Eng. Sci.*, *22*, 847–853.

Fredsoe, J. (1993), Modelling of non-cohesive sediment transport processes in the marine environnment, *Coastal Eng.*, *21*, 71–103.

Gidaspow, D. (1994), *Multiphase Flow and Fluidization*, Academic, San Diego, Calif.

Gore, R. A., and C. T. Crowe (1989), Effect of particle size on modulating turbulent intensity, *Int. J. Multiphase Flow*, *15*, 279–285.

Graham, A. L. (1981), On the viscosity of suspensions of solide spheres, *Appl. Sci. Res.*, *37*, 275–286.

Greimann, B., and F. Holly (2001), Two-phase flow analysis of concentration profile, *J. Hydraul. Eng.*, *127*, 753–761.

Greimann, B. P., M. Muste, and F. M. Holly Jr. (1999), Two-phase formulation of suspended sediment transport, *J. Hydraul. Res.*, *37*, 479–500.

Guillou, S., and K. D. Nguyen (1999), An improved technique for solving two-dimensional shallow water problems, *Int. J. Numer. Methods Fluids*, *29*, 465–483.

Guillou, S., N. Barbry, and K. D. Nguyen (2000), Calcul numérique des ondes de surface par une méthode de projection et un maillage eulérien adaptatif, *C.R. Acad. Sci. Ser. IIb Mec. Phys. Astron.*, *328*, 875–881.

Haider, A., and O. Levenspiel (1989), Drag coefficient and terminal velocity of spherical and non-spherical particles, *Powder Technol.*, *58*, 63–70.

Harlow, F. H., and J. E. Welch (1965), Numerical calculation of time-dependant viscous incompressible flow of fluid with free surface, *J. Phys. Fluids*, *8*, 2182–2189.

Hetsroni, G. (1989), Particles-turbulence interaction, *Int. J. Multiphase Flow*, *15*, 735–746.

Hsu, T., J. T. Jenkins, and P. L.-F. Liu (2003), On two-phase sediment transport: Dilute flow, *J. Geophys. Res.*, *108*(C3), 3057, doi:10.1029/2001JC001276.

Ishii, M. (1975), *Thermo-Fluid Dynamic Theory of Two-Phase Flow*, Eyrolles, Paris.

Jenkins, J. T., and M. W. Richman (1985), Grad's 13-moment system for a dense gas of inelastic spheres, *Arch. Ration. Mech. Anal.*, *87*, 355–377.

Kaftori, D., G. Hestroni, and S. Banerjee (1996), Particle behavior in the turbulent boundary layer. Velocity and distribution profiles, *Phys. Fluids*, *7*, 1107–1121.

Lundgren, T. (1972), Slow flow through stationary random beds and suspensions of spheres, *J. Fluid Mech.*, *51*, 273–299.

Ma, D., and G. Ahmadi (1986), An equation of state for dense rigid sphere gases, *J. Chem. Phys.*, *84*, 3449–3450.

Ma, D., and G. Ahmadi (1988), A kinetic model for rapid granular flows of nearly elastic particles including interstitial fluid effects, *Powder Technol.*, *56*, 191–207.

Mohammadi, B., and O. Pironneau (1994), *Analysis of the K-ε Turbulence Model*, John Wiley, Chichester, U.K.

Muste, M., and V. C. Patel (1997), Velocity profiles for particles and liquid in open-channel flow with suspensded sediment, *J. Hydraulic. Eng.*, *123*, 742–751.

Muste, M., K. Yu, I. Fujita, and R. Ettema (2005), Two-phase versus mixed-flow perspective on suspended sediment transport in turbulent channel flows, *Water Resour. Res.*, *41*, W10402, doi:10.1029/2004WR003595.

Nezu, I., and W. Rodi (1986), Open channel flow measurement with laser-dopler anemometer, *J. Hydraul. Eng.*, *112*, 335–355.

Orlanski, I. (1976), A simple boundary condition for unbounded hyperbolic flows, *J. Comput. Phys.*, *21*, 251–269.

Peirano, E., and B. Leckner (1998), Fundamentals of turbulent gas-solid flows applied to circulating fluidized bed combustion, *Prog. Energy Combust. Sci.*, *24*, 259–296.

Rashidi, M. G., G. Hetsroni, and S. Banerjee (1990), Particle-turbulence interaction in a boundary layer, *Int. J. Multiphase Flow*, *16*, 935–949.

Raudkivi, A. J. (1998), Keynote lecture: Loose boundary hydraulic-grey zones, in *River Sedimentation: Theory and Applications, Proceedings of the Seventh International Symposium on River Sedimentation*, edited by A. W. Jayawardena, J. H. W. Lee, and Z. Y. Wang, pp. 15–33, A. A. Balkema, Brookfield, Vt.

Rouse, H. (1937), Modern conceptions of the mechanics of turbulence, *Trans. Am. Soc. Civ. Eng.*, *102*, 463–505.

Simonin, O. (1991), Prediction of the dispersed phase turbulence in particle-laden jets, in *Gas-Solid Flows*, *FED Ser.*, vol. 121, pp. 197–206, Am. Soc. Mech. Eng., New York.

Simonin, O., and P. L. Viollet (1990), Numerical study on phase dispersion mechanisms in turbulent bubbly flows, in *Fifth Workshop on Two-Phase Flow Predictions*, edited by M. Sommerfeld and D. Wennerberg pp. 156–166, Forsch. Jülich, Jülich, Germany.

Smith, J. D., and S. R. McLean (1977), Spatially averaged flow over a wavy surface, *J. Geophys. Res.*, *82*, 1735–1746.

Sumer, B. M., and R. Deigaard (1981), Particles motions near the bottom in turbulent flow in an open channel: Part 2, *J. Fluid Mech.*, *109*, 311–337.

Tchen, C. M. (1947), Mean value and correlation problems connected with the motion of small particles suspended in a turbulent fluid, Ph.D. thesis, Delft Univ. of Technol., Delft, Netherlands.

Temam, R. (1969), Sur l'approximation des équations de Navier-Stokes par la méthode des pas fractionnaires (II), *Arch. Ration. Mech. Anal.*, *26*, 367–380.

Van Rijn, L. C. (1984), Sediment transport, part II: Suspended load transport, *J. Hydraul. Eng.*, *110*, 1613–1641.

Vilaret, C., and A. G. Davies (1995), Modelling of sediment-turbulent flow interactions, *Appl. Mech. Rev.*, *48*, 601–609.

Wells, M. R., and D. E. Stock (1983), The effects of crossing trajectories effects on the dispersion of particles in a turbulent flow, *J. Fluid Mech.*, *9*, 421–435.

J. Chauchat, Laboratoire de Morphodynamique Continentale et Côtière, UMR6143, Université de Caen, 24 rue des Tilleuls, F-14000 Caen, France. (julien.chauchat@unicaen.fr)

S. Guillou, LUSAC, EA 2607, Ecole d'Ingénieurs de Cherbourg, Université de Caen, BP 78, F-50130, Octeville, France. (sylvain.guillou@unicaen.fr)